ROCK PHYSICS CHARACTERIZATION OF POTENTIAL RESERVOIRS AND SEALS FOR CO2 STORAGE, OFFSHORE SOUTHEASTERN U.S.

By

ANDREW J. BEAN

Bachelor of Science in Geology

Bachelor of Arts in Geography

West Virginia University

Morgantown, WV

2016

Submitted to the Faculty of the
Graduate College of the
Oklahoma State University
in partial fulfillment of
the requirements for
the Degree of
MASTER OF SCIENCE
July, 2020

ROCK PHYSICS CHARACTERIZATION OF

POTENTIAL RESERVOIRS AND SEALS FOR

CO2 STORAGE, OFFSHORE SOUTHEASTERN U.S.

Thesis Approved:

Dr. Camelia Knapp

Thesis Adviser

Dr. James Knapp

Dr. Jack Pashin

ACKNOWLEDGEMENTS

This thesis is the product of great collaboration and teamwork, and I would like to acknowledge every individual who assisted in making this possible. Above all others, I would like to sincerely thank my advisor, Dr. Camelia Knapp, for treating me as more than a student. Since AGU 2016 in San Francisco to the onset of my studies in Columbia, SC and ultimately through the transitions to Stillwater, OK, she has provided constant support and made me feel like an honorary member of the Knapp family. I would also like to thank my other committee members, Dr. Jim Knapp and Dr. Jack Pashin for being there to answer questions and point me in the right direction when looking for resources. The transition from University of South Carolina to Oklahoma State University did not come easy, so I would like to extend my appreciation to Dr. Mohamed Abdel-Salam for being an outstanding graduate coordinator and always being available at any moment to help navigate confusing Graduate College paperwork, and Sandy Earls for facilitating the many travel and paperwork issues throughout my two years at OSU.

I would also like to give a shout-out to the entire Boone Pickens School of Geology family. Each and every one of you helped ease the anxiety of switching graduate schools and welcomed the UofSC students with open arms. This is especially true for those in The Tribe. Thank you to Seyi Sholanke, Alejandra Santiago Torres, and Estefanny Dávalos for being caring, trustworthy, down-to-earth human beings.

This research wouldn't have been possible without funding provided by the U.S. Department of Energy's National Energy Technology Laboratory (NETL) through project FE0026086. Thank you to the Southeast Offshore Storage Resource Assessment (SOSRA) team and the Southern States Energy Board (SSEB) for financially supporting this project. I personally would like to acknowledge Dr. Peter McLaughlin and Mojisola KunleDare at the Delaware Geological Survey for allowing this rare core to be examined. The experiments in this study would not have been conducted if not for Dr. Dustin Crandall, Justin Moore, Rick Spaulding, and the Geoimaging and Characterization crew at NETL-MGN. Your gracious accommodation and guidance throughout this study will not be forgotten.

Most importantly, I would like to extend my gratitude to my bottomless source of moral and emotional support, beginning with the love of my life, Gokce Astekin. Surviving the stress of graduate school, and life as a whole, is much easier when you're a part of a duo. Lastly, thank you greatly to my family and friends for sticking with me through my circuitous journey. Every time I thought I hit a dead-end, you convinced me that it was only a speed bump. I love you all.

Name: ANDREW J. BEAN

Date of Degree: AUGUST, 2020

Title of Study: ROCK PHYSICS CHARACTERIZATION OF POTENTIAL RESERVOIRS AND SEALS FOR CO2 STORAGE, OFFSHORE SOUTHEASTERN U.S.

Major Field: GEOLOGY

Abstract:

Geologic carbon sequestration is emerging as a viable method to curb anthropogenic CO2 emissions. With 40% of the United States' total CO2 emissions originating in the Southeast, proximal geologic storage sites are being characterized to reduce the region's carbon footprint. Funded by the Department of Energy, this multi-study project aims to estimate the CO2 storage potential for the 11,000 mi^2 Southeast Atlantic Continental Margin (SE-ACM). Previous studies in this geologic region generated a velocity model, interpreted 2D seismic and wireline data, recommended prospective reservoirs and seals, and quantified upwards of 817 Gt of storage potential within the Upper Cretaceous, Lower Cretaceous, and Upper Jurassic formations of the SE-ACM. This research project serves to ground-truth previous findings using the only drill core in the region to mechanically characterize prospective reservoirs and seals, determine seal integrity, and refine previous estimates of storage potential with dynamic geomechanical testing and high-resolution computed tomography (CT) scanning.

An optimized workflow was designed around remaining COST GE-1 core and stipulations set by the Delaware Geological Survey to maximize data generation while also minimizing destructive analyses to preserve this rare core. Non-destructive medical CT scanner, industrial CT scanner, and multi-sensor core logger were utilized on whole core. Plugs were sampled at selected depths for porosity, permeability, and dynamic geomechanical testing. Analysis identified a positive relationship between CT number and wireline bulk density. Porosity values were used to develop a methodology to quantify interconnected porosity using 3D industrial CT scans. Finally, mechanical testing generated velocities and elastic moduli to help characterize an "auxetic" rock. With these analyses, reservoir-specific interconnected porosity values were used to refine and constrain CO_2 efficiency factors. It was also recommended to revisit calculations for reservoir thickness across the SE-ACM due to apparent heterogeneity in proposed reservoir intervals. Using velocities and lithological information, seal integrity was plotted for four proposed seal intervals. The SE-ACM has great potential for CO_2 storage but could benefit from additional data acquisition to improve upon previous assessments of storage volume, assess lateral continuity of seals and reservoirs, and demonstrate permanence.

TABLE OF CONTENTS

Chapter Page

LIST OF TABLES

Table Page

LIST OF FIGURES

Figure Page

CHAPTER I

INTRODUCTION

Carbon Capture and Storage Overview

Carbon capture and storage (CCS) is a technology capable of capturing anthropogenic carbon dioxide (CO_2) created at large point sources, transporting it safely, and geologically sequestering it to inhibit emission into the atmosphere. With industry and power generation comprising 50% of total U.S. greenhouse gas emissions in 2018 (EPA, 2018), CCS has already garnered attention as an approach to combat anthropogenic climate change and ensure access to current and future carbon-neutral energy demand. To further spur interest and increase economic incentive within private industry, the United States Treasury Department released the 45Q tax credit program in 2018 which states that projects demonstrating durable storage of CO_2 will receive a credit of $50 per metric ton of CO_2 (DOE, 2019). Taking advantage of these motivations, ten CCS facilities are currently operating across the country with a combined capture capacity of greater than 25 million metric tons per year. In addition, seventeen additional CCS facilities are under development (Beck, 2019). Overall, CCS technology is picking up steam in the U.S.

Prior to geologic storage of CO_2, potential injection locations undergo site screening. A potential site requires an outreach plan to the public and stakeholders, acquiring and analyzing geological and geophysical data, updating and refining of models, and land permitting. If

outreach activities and permitting are successful, and geologic data and models support further development, then detailed characterization is initiated (NETL, 2017). During characterization, surface and subsurface geological and geophysical data are used to better understand prospective reservoirs, seals, traps, presence of conduits for leakage such as faults, and volumetric estimates. Currently, the U.S. Department of Energy (DOE) is funding research for and investigating five types of underground formations including saline formations, oil and natural gas reservoirs, unmineable coal seams, organic-rich shales, and basalt formations (NETL, 2017). Volumetrics can be calculated specifically for the formation type and can be accomplished by using the equation for mass CO_2 storage (G_{CO2}) (Goodman, 2016):

$$G_{CO2} = A_t * h_g * \varphi_{tot} * \rho * E \quad \text{[Eqn. 1]}$$

where A_t = total area of reservoir, h_g = gross thickness of reservoir, φ_{tot} = total porosity in reservoir volume, ρ = density of CO_2 at storage conditions, and E = CO_2 storage efficiency factor.

An important component of G_{CO2} equation, and the primary focus of this study, is the storage efficiency factor, E. In an open system, E specifies the portion of rock amenable for CO_2 storage and the fraction of pore space where injected CO_2 can permanently displace formation fluids (NETL, 2017). Values for E are intended to be reservoir-specific variables but can be estimated by using Monte Carlo simulations if reservoir data is lacking. Thus, the efficiency factor can be fine-tuned for the specific type of prospective reservoir. The choice of which efficiency factor to apply depends on the area, thickness, porosity, and pressure boundary conditions of the formation. According to Goodman 2016, misapplications of the efficiency factors are common and may lead to under- or overestimation of effective storage potential. For saline formations, the individual factors of E_{saline} can be broken down into:

$$E_{saline} = E_A E_h E_\varphi E_v E_d \quad \text{[Eqn. 2]}$$

where E_A = net-to-total area, E_h = net-to-gross thickness, and E_φ = effective-to-total porosity are the geologic variables (IEA GHG, 2009), and E_v = volumetric displacement efficiency, and E_d = microscopic displacement efficiency. Ideally, using known reservoir data to calculate an efficiency factor value can lead to a more precise estimation of storable volume for CO_2.

Numerous CO_2 injection sites across the globe have demonstrated long-term permanence of a high volume of CO_2 captured at anthropogenic point sources. The Sleipner project, which is operated by Equinor, began in 1996 and was the world's first commercial CO_2 storage project. The Sleipner West field produces hydrocarbons as well as up to 9% CO_2 as a byproduct from the 3000 ft subsea saline Utsira Formation. Instead of the CO_2 escaping into the atmosphere, it is injected back into the producing formation while the hydrocarbons are pipelined to market. Had the CO_2 not been injected and instead released into the atmosphere, Equinor would need to pay additional Norwegian taxes. Every year at Sleipner, 1 million metric tons of CO_2 are returned to geologic storage (Schrag, 2009).

A few favorable circumstances contributed to the success of Sleipner. The location of injection is the same as the source of the CO_2. This means that virtually no additional infrastructure, such as CO_2 pipelines, were necessary. Additionally, because the injection reservoir is a proven accumulation of entrapped hydrocarbons, it has demonstrated long-term permanence with no evidence of CO_2 leakage. The Sleipner site also benefits from being offshore with no apparent risk to leakage into an underground source of drinking water (USDW), which is an inherent risk to onshore injection sites.

Another notable CCS project is the CarbFix program in Iceland. In a process that can take thousands of years to accomplish, CarbFix demonstrated mineralization of 90% of injected CO_2 into calcite over a two-year period (Pogge von Strandman, 2019). Contrastingly to Sleipner, CarbFix capturing CO_2 at geothermal power plants and targeting basalt formations onshore. In

total, the results from the CarbFix program suggest that approximately 200 metric tons of CO_2 were injected, resulting in permanent mineralization of 165 tons (Pogge von Strandman, 2019). Although the total volume of injected CO_2 at CarbFix pales in comparison to Sleipner, this project proves that even low permeability basalts are permanent storage options. Similar to Sleipner, the CarbFix project also benefited from having the necessary infrastructure in place to capture and inject CO_2, and thus was economically viable.

Motivation for CCS in Southeast United States

The southeastern region of the United States, defined by the American Association of Geographers, is comprised of Alabama, Florida, Georgia, Kentucky, Mississippi, North Carolina, South Carolina, Tennessee, Maryland, Virginia, and West Virginia. The Southeast is a hotspot for industrial sources of CO_2 (seen in Figure 1); as of 2017 the Southeast generates approximately one quarter of total CO_2 emissions in the U.S. (1177 million metric tons) (EPA, 2019). According to the United States Department of Agriculture, the comprehensive geological assessment of this region is vital to the success of CCS in the U.S. (Mitchell, 2013). Despite this fact, much of the Southeast remains under-assessed and many states lack proximal proven geologic formations onshore that are capable of storing CO_2.

For the eastern-most states of the region, eyes have shifted offshore for viable geologic storage of CO_2 for good reason. In the DOE-funded Southeast Offshore Storage Resource Assessment (SOSRA) study of offshore Alabama and western Florida covering 10,000 mi^2, Hills and Pashin (2010) approximated a combined 200 gigatons (Gt) of potential CO_2 storage in Miocene and Cretaceous reservoirs. In another SOSRA study spanning the 11,000 mi^2 offshore region from the southern tip of Florida to the northernmost portions of South Carolina, an estimated 32 Gt of carbon storage potential exists in Upper Cretaceous units (Almutairi, 2018). In a recent resource assessment of the 66,000 mi^2 mid-Atlantic shelf of states including Virginia,

Maryland, Delaware, New York, and New Jersey, Fukai et al. estimated between 37-403 Gt of prospective CO_2 storage resources. Tremendous storage potential has been estimated to exist in the offshore Southeast U.S..

In addition to storage potential, offshore sites in federal waters offer advantages to onshore sites regulated by individual states. Increased subsurface pressures due to CO_2 injection can displace formation fluids from the reservoir. In onshore scenarios these need to be properly disposed of due to high concentrations of toxic metals. However, formation fluid in offshore settings has chemistry comparable to seawater, as it is essentially ancient seawater modified by diagenetic reactions. As long as it does not contain high concentrations of hydrocarbons, the release of formation fluid into seawater does not cause harm to marine environments (Schrag, 2009).

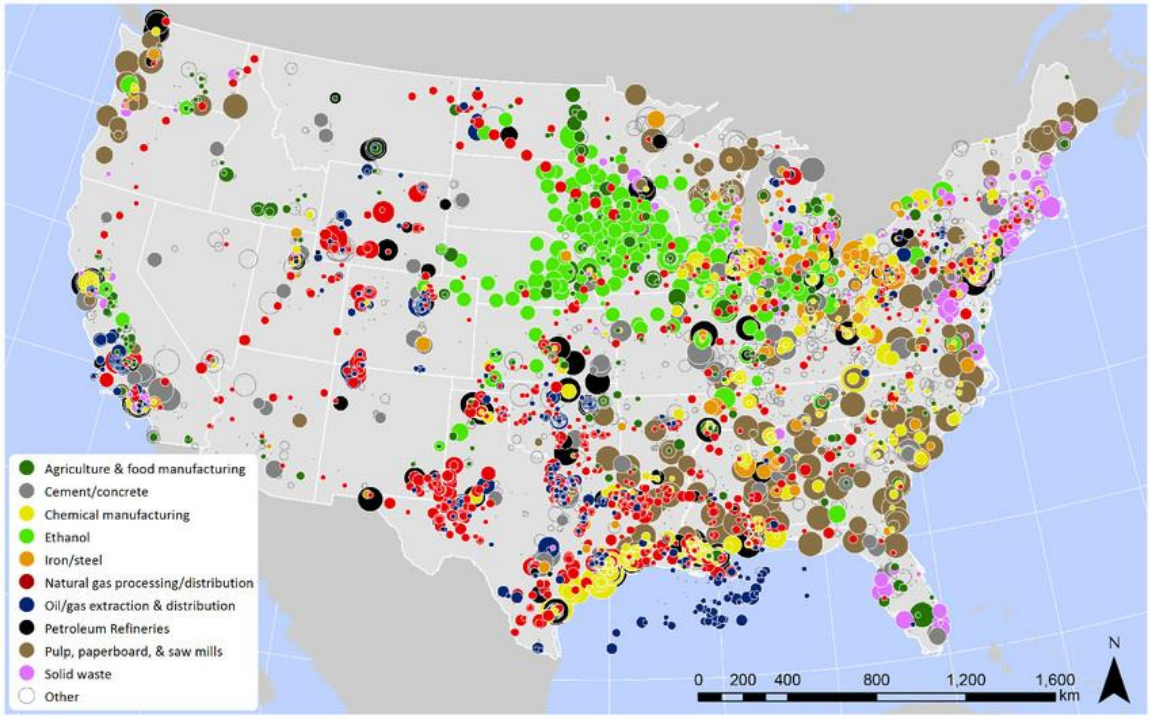

Figure 1. Locations of 6,226 industrial CO2 sources across the contiguous U.S. Sources emitting <25 ktCO2 (2,471 facilities) are shown as small grey dots. Circles are sized proportional to CO2 emissions ranging from 25-50 kt CO2 (smallest circles) to 5-10.5 Mt CO2 per yr (largest circle). Power plants are not shown. (Middleton 2017).

Beyond the technical advantages, there are various socio-political and economic reasons why offshore CO_2 storage is essential in early deployment of CCS technology. Selecting sites close to populated areas near point sources of CO_2 may be unlikely due to regulation, public opposition, or fear of potential contamination to USDW. In contrast, offshore sites are located far offshore. CO_2 injection beneath the ocean floor is the most optimal solution for large coastal population centers.

Previous and Current SOSRA Research in the Southeastern Atlantic Continental Margin

As a continuation of SOSRA, managed by the Southern States Energy Board (SSEB), it is important to place this study into the context of past and current SOSRA research. This study, as well as those mentioned below, focused their research within the 11,000 mi^2 of offshore continental shelf spanning northern South Carolina to the southern tip of Florida, or the Southeastern Atlantic Continental Margin (SE-ACM).

Almutairi (2018) conducted the first resource assessment of this region for offshore CO_2 storage resources. His research focused solely on Upper Cretaceous strata and utilized legacy 2-D seismic reflection and well data to create structure and thickness maps for potential reservoirs and seals on a local and regional scale. Almutairi also conducted seismic inversion to discriminate lithology and predict porosity regimes. Ultimately, five reservoirs and seals were selected as candidates with porosity values of 20-30%, permeability of 1-447 millidarcies (mD), and CO_2 storage volumetrics estimated to be approximately 32 Gt for Upper Cretaceous units.

Ollmann (2018) developed a velocity model to convert legacy 2-D seismic reflection data to depth using 50,000 previously published stacking velocities. Using this velocity model, thicknesses were estimated and storage potential of CO_2 reservoirs were updated.

Almayahi (*in prep*) is conducting a resource assessment for offshore CO_2 storage resources but focusing solely on Lower Cretaceous to Basement strata. Legacy 2-D seismic and

well log data are being analyzed to create isopachs of potential reservoirs and seals. Although volumetric calculations are preliminary, Almayahi identified several potential reservoir and seal intervals within the Lower Cretaceous and Upper Jurassic.

Alshammari (*in prep*) is focusing on injection simulation modeling. Models were generated demonstrating 73 million m^3 per year injection rates in order to predict permeability and porosity values, estimate the probability of CO_2 leakage from overpressure, calculate geomechanical properties such as Young's modulus, and predict mineralization scenarios.

Research Objectives

Previous research in the SE-ACM focused primarily on seismic and well log interpretation and evaluation. This study hopes to supplement past work by conducting experimental analyses on available drill core in the SE-ACM. The primary objective of this study is to ground-truth previous findings by collecting data on rock properties such as porosity, permeability, density and performing dynamic geomechanical testing to collect data on elastic moduli, P-wave, and S-wave velocities. Using the geomechanical data, this study also aims to identify a methodology of quantifying interconnected porosity in proposed reservoir intervals to constrain the effective-to-total porosity efficiency factor, E_φ, in Equation 2. This experimentally derived value will lead to a more precise estimate of total CO_2 storage volume, G_{CO2}, in Equation 1. Finally, the last goal of this study is to assess seal integrity of proposed seal intervals using the newly-collected geomechanical data. Ultimately, collecting these new core-derived data will provide a better understanding of CO_2 storage potential in the offshore southeastern U.S..

CHAPTER II

STUDY AREA

Geologic Setting

The tectonic history of the SE-ACM began following the Alleghenian orogeny and the collision of Laurentia with Gondwana. This was succeeded by continental rifting in the Early Mesozoic during the breakup of Pangaea. This resulted in localized tectonic subsidence in restricted extensional basins, which was followed a period of thermal subsidence which continues today (Dillon, 1988).

In most passive margins, stratigraphic sequences can be classified as being laterally extensive and continuous with little to no structural disruption. The oldest post-rift sediments in the region are Jurassic in age and lie above the regional unconformity, known as the "post rift unconformity". These Jurassic sediments originate from rapid clastic sedimentation, succeeded by evaporite deposition, and followed by a widespread deposition of shallow water carbonate with periodic terrigenous influx (Dillon, 1988). The thickness of the Jurassic section is suggested to be 4.6 miles, and thickening seaward (Dillon, 1977). The overlying Cretaceous section transitions from more clastic sedimentation in the North to increasing carbonate deposition in the South. This created a large carbonate platform spanning the Blake Plateau province. The Suwanee Strait, which evolved over time into the modern-day Gulf Stream, supplied the Upper Cretaceous interval with clastic material, which created a distinct facies change to the nearby Bahama Bank

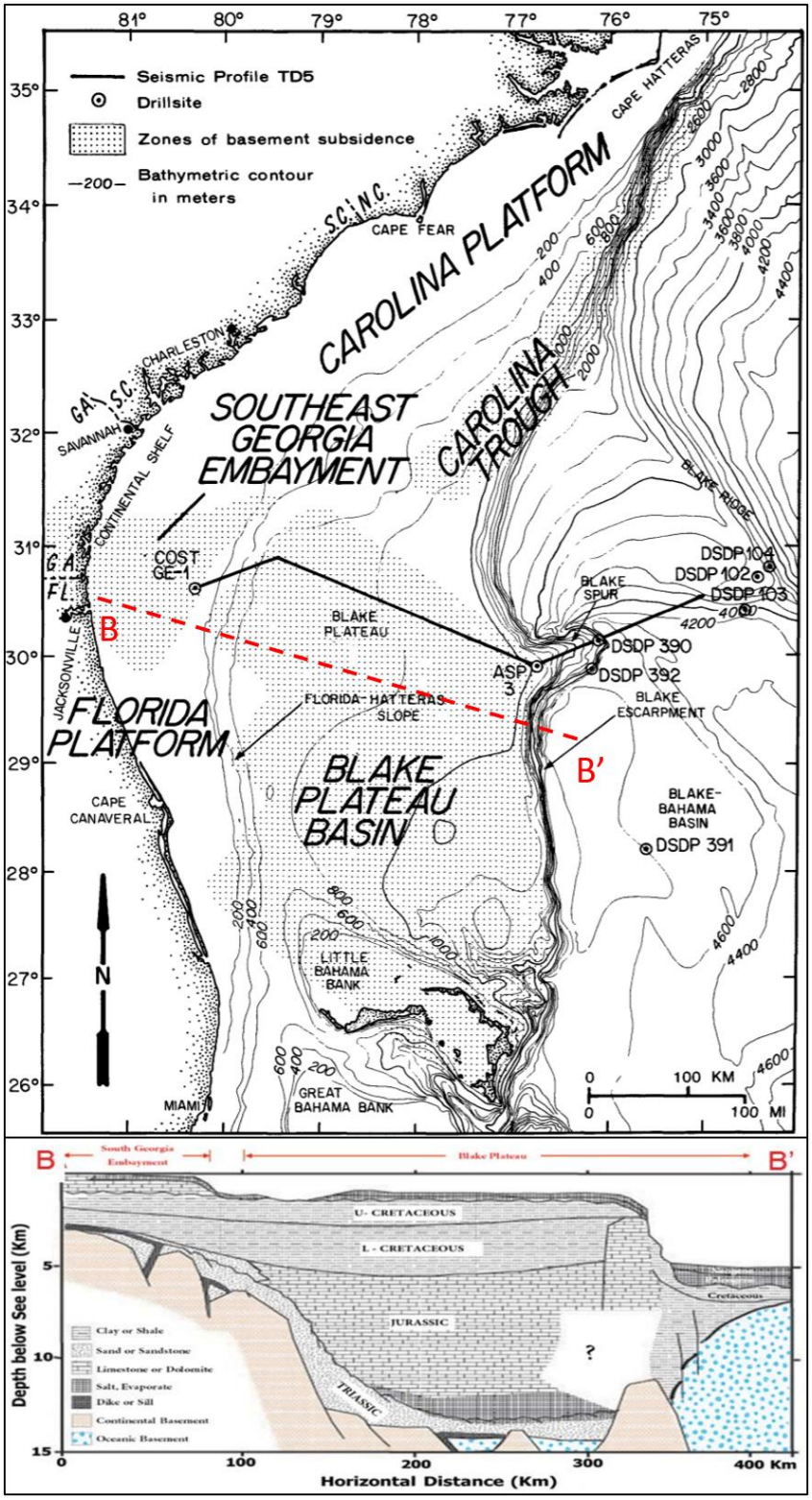

Figure 2. [Top] Geologic provinces and bathymetric features across the SE-ACM, in relation to the COST GE-1 well, USGS seismic line TD-5 in black, and profile BB' in red (modified from Scholle, 1979). [Bottom] Profile BB' displaying depths of the Southeast Georgia Embayment and Blake Plateau provinces (modified from Poag, 1978).

and Florida Platform (Pinet, 1985). Sedimentation in the Upper Cretaceous and Cenozoic sections were controlled by strong paleocurrents across the SE-ACM, which eroded much of the Paleogene sediments and inhibited further deposition off the Florida-Hatteras slope. The primary areas of deposition that remained occurred in the Southeast Georgia Embayment, the Blake Plateau Basin, and the Carolina Trough with sediment thicknesses ranging from 10,000-23,000 feet (Maher, 1971). Figure 2 displays the locations of these provinces in relation to the Southeast Georgia Embayment and the COST GE-1 well, which will be the focal area of this study.

The largest structural feature within the Florida-Hatteras shelf is the Southeast Georgia Embayment. It is an eastward-plunging extensional depression, but is dwarfed by other sedimentary basins in the SE-ACM. Core from the COST GE-1 well indicates that Paleozoic rocks occur at a depth of 10,560 feet, overlain by Jurassic non-marine clasts with interbedded units of anhydrite, coal, and dolomite. This sedimentary sequence dominates through the Mesozoic, but transitions into carbonate deposition in the Cretaceous. The Southeast Georgia Embayment is likely undergoing sedimentation to this day (Dillon, 1977).

Data Coverage

The SE-ACM region is well covered by 160,000 km of legacy 2D seismic reflection data, as seen in Figure 3. These data were generated during the 1970's and 1980's as part of an offshore exploration phase for petroleum. They are publicly available through the Bureau of Ocean Energy Management (BOEM) and United States Geological Survey (USGS). All exploration wells drilled within the SE-ACM are located within the Southeast Georgia Embayment. Each well has an associated well report, however only three wells contain sonic logs, making them integrable with seismic data. Each well produced drill cuttings, from which thin sections and slides were made to observe palynology, nannofossils, and kerogen. However, the only well with existing,

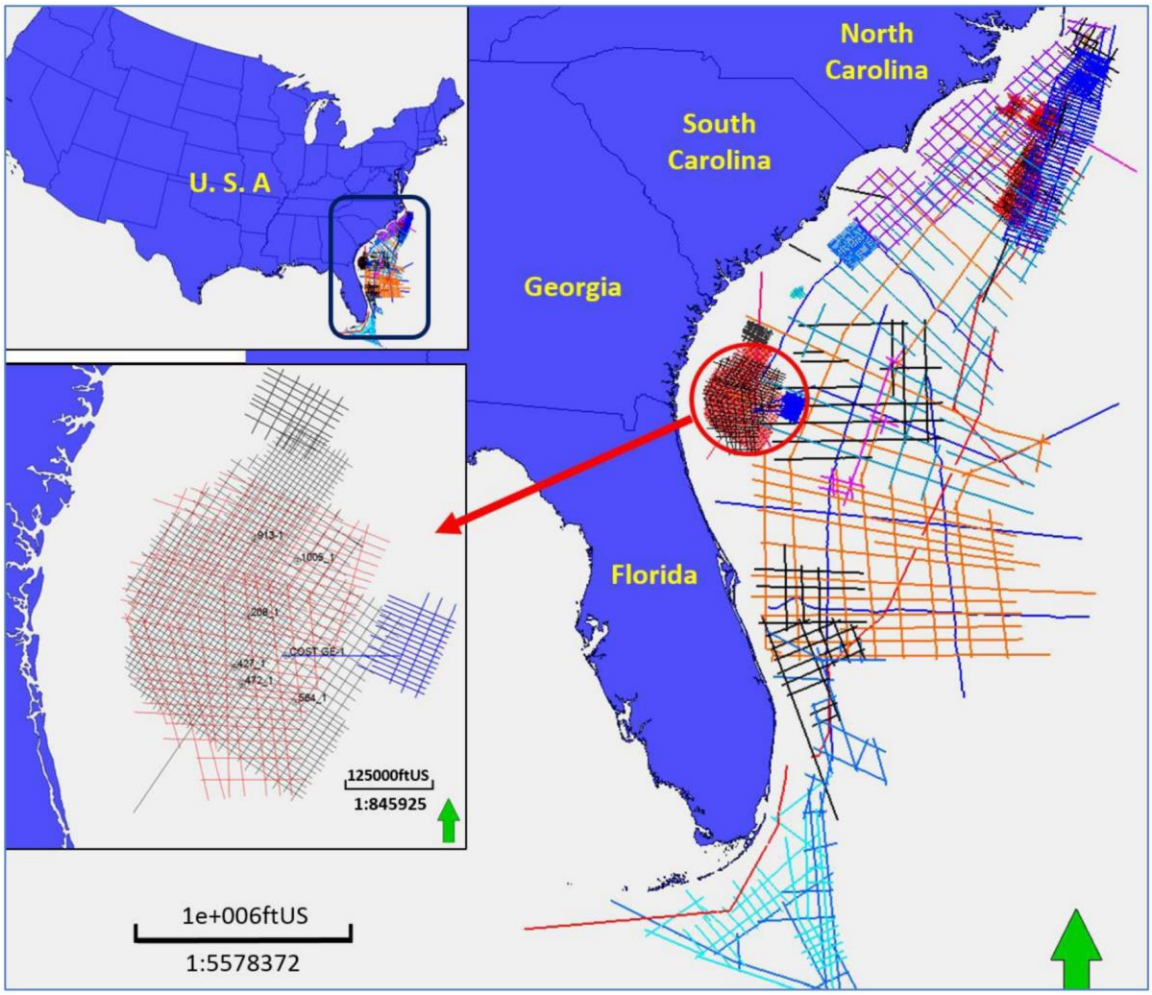

Figure 3. Map of legacy 2-D seismic reflection data across the SE-ACM. The red circle denotes the location of a high-density seismic survey and seven exploration wells within the Southeast Georgia Embayment (Almutairi, 2018).

intact core is COST GE-1. All remaining drill core, drill cuttings, and derivative slides and thin sections are curated by the Delaware Geological Survey (DGS).

Scope of Study

This study depended on availability of intact drill core in the SE-ACM. Currently, the COST GE-1 well is the only well drilled in the region with associated core. The well was drilled to a depth of 13,254 feet below sea level, and 15 intervals (375 total feet) were cored during drilling. Out of this total, roughly 335 feet were recovered (Scholle, 1979). DGS, curator of

COST GE-1 drill core, maintains a comprehensive inventory listing the remaining core in its possession. Currently, only 320.8 total feet of core remain for the 11,000 mi^2 SE-ACM region (Table 1). The scope of this study was further narrowed using proposed seal and reservoir intervals from Almutairi (2018) and preliminary intervals from Almayahi (*in prep*). If core existed for a proposed interval, then this section was selected for analysis, as denoted in green rows in Table 2. This limited the study to analysis within the Lower Cretaceous and Upper Jurassic intervals only.

Remaining Core Interval (ft)	Interval Thickness (ft)
3024-3033	9
3036-3054	18
6607-6619.5	12.5
6619.9-6655.4	35.5
7040-7087	47
7091-7098.9	7.9
8331-8346	15
8349-8379	30
8382-8390.8	8.8
9453-9506.1	53.1
10520-10566.1	46.1
11357-11387	30
11635.5-11642.6	7.1
13252-13252.8	0.8
Total Depth of Core (ft)	
320.8	

Table 1. A list of remaining COST GE-1 drill core in the DGS collection, the depths, and the thickness of each interval. All depths are in Kelly Bushing.

Geologic Age (source)	Proposed	Top Depth (ft)	Bottom Depth (ft)	Available Core?
Upper Cretaceous (Almutairi, 2018)	Seal	3500	3570	No
	Reservoir	3570	3750	No
	Seal	3750	4000	No
	Reservoir	4020	4170	No
	Seal	4170	4250	No
	Reservoir	4360	-	No
	Seal	4400	5500	No
	Reservoir	5400	5580	No
	Seal	5580	5720	No
	Reservoir	5720	5950	No
Lower Cretaceous (Almayahi, *in prep*)	Seal	5840	5988	No
	Reservoir	5988	6520	No
	Seal	6520	6900	Yes
	Reservoir	6900	7200	Yes
	Seal	7200	7360	No
	Reservoir	7360	8665	Yes
Upper Jurassic (Almayahi, *in prep*)	Seal	8240	8708	Yes
	Reservoir	8708	9100	No
	Seal	9100	9300	No
	Reservoir	9300	9790	Yes
	Seal	9790	10710	Yes
	Reservoir	10710	10800	No
	Seal	10800	11200	No

Table 2. Proposed intervals for seals and reservoirs in the Upper Cretaceous (Almutairi, 2018), and Lower Cretaceous and Upper Jurassic (Almayahi, in prep). Available core within an interval is denoted with "Yes" and a green row, while lack of core is displayed as "No" and a red row. All depths are in Kelly Bushing.

CHAPTER III

DATA COLLECTION

Workflow

Given the scarcity of drill core in the SE-ACM region, several stipulations were set by DGS and agreed to prior to loaning samples of COST GE-1 core. A workflow was developed to maximize data generation from this rare core in a non-destructive manner in order to ensure safe return of minimally altered samples to DGS. When selecting a site to conduct experimental analyses, the risk of damaging core during shipping was also considered. Ultimately, the Department of Energy's National Energy Technology Laboratory (NETL) in Morgantown, WV (NETL-MGN) and Pittsburgh, PA (NETL-PGH) was selected to perform these experiments. NETL-MGN and NETL-PGH are home to cutting edge, non-destructive computed tomography (CT) and core logging technology, as well as equipment capable of dynamic geomechanical testing, within a day's drive from DGS in Newark, Delaware. This allowed for safe transportation of the core by personal vehicle instead of risking damage using commercial shipping. All experiments detailed in this study were conducted and performed by federal researchers and contractors at NETL who are trained on the specific equipment used. Data collection was performed around researchers' schedules over a three-week period to minimize machine downtime and project delays to ongoing projects at NETL.

The workflow of analyses can be seen in Figure 4. Of the 320.8 total feet of ¾-slabbed

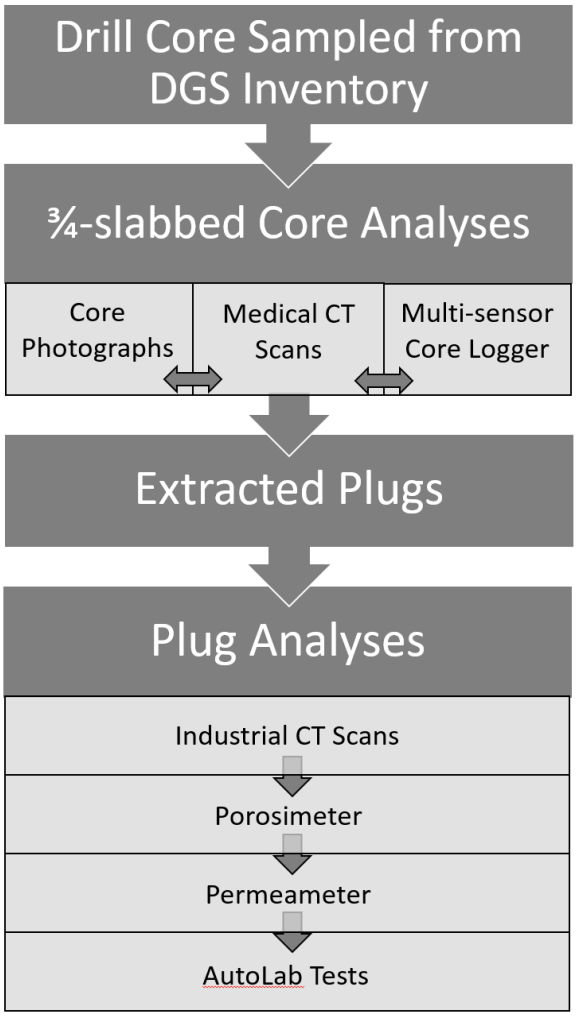

Figure 4. Workflow of data collection, beginning at the top. Horizontal arrows indicate concurrent experiments. Vertical arrows indicate succession.

Depth Intervals (ft)	Number of Core Boxes	Sample Types (as listed in DGS Inventory)
6607-6614	3	Slabbed Core
6647.5-6655.4	4	
7040-7048	3	
7091-7098.9	3	
8352-8361	3	
9453-9460.9	3	
9501.8-9506.1	2	
10545.9-10551	2	
Total Depth of Core (ft)	**Total Number of Core Boxes**	
57.1	23	

Table 3. Depth intervals sampled from the DGS inventory.

core available in the DGS inventory, 57.1 feet were sampled from the collection (Table 3). After sampling, the core was transported to NETL-MGN. All depths henceforth are in Kelly Bushing (KB).

Core Photographs

Upon arrival to NETL-MGN, all depth intervals were immediately captured in high-resolution, white light photography with a digital single-lens reflex (DSLR) camera. These photos can be seen in Appendix B.

Medical Computed Tomography

Medical CT scans began almost immediately upon arrival and concurrently with camera photography and multi-sensor core logging. Core remained in its original 3-foot long cardboard packing and was scanned beginning with the shallowest depth interval. No sample preparation was necessary. The scanner used was a medical Toshiba® Aquilion RXL™ Multislice Helical Computed Tomography Scanner, seen in Figure 5. It produces 0.35-0.55 millimeter resolution greyscale tagged image file (TIF) in a non-destructive manner. The variation in greyscale values indicate variations in CT number, which is directly proportional to changes in attenuation and bulk density of the rock (NETL, 2017). Output TIF files totaled 238 MB in volume, were named by their respective depths, and were essential in optimizing plug sample depths.

Multi-Sensor Core Logger

Another non-destructive method used to obtain COST GE-1 core geophysical and rock properties was the Geotek® Multi-Sensor Core Logger (MSCL) system, seen in Figure 6. All depth intervals of core were removed from its containing box, three feet at a time, and placed onto a stationary track. Once in position, sensors autonomously move across the core taking measurements for core thickness, P-wave velocity, gamma density, fractional porosity, magnetic

Figure 5. Image of the medical CT scanner utilized onsite at NETL-MGN. From National Energy Technology Laboratory Flickr profile (2015).

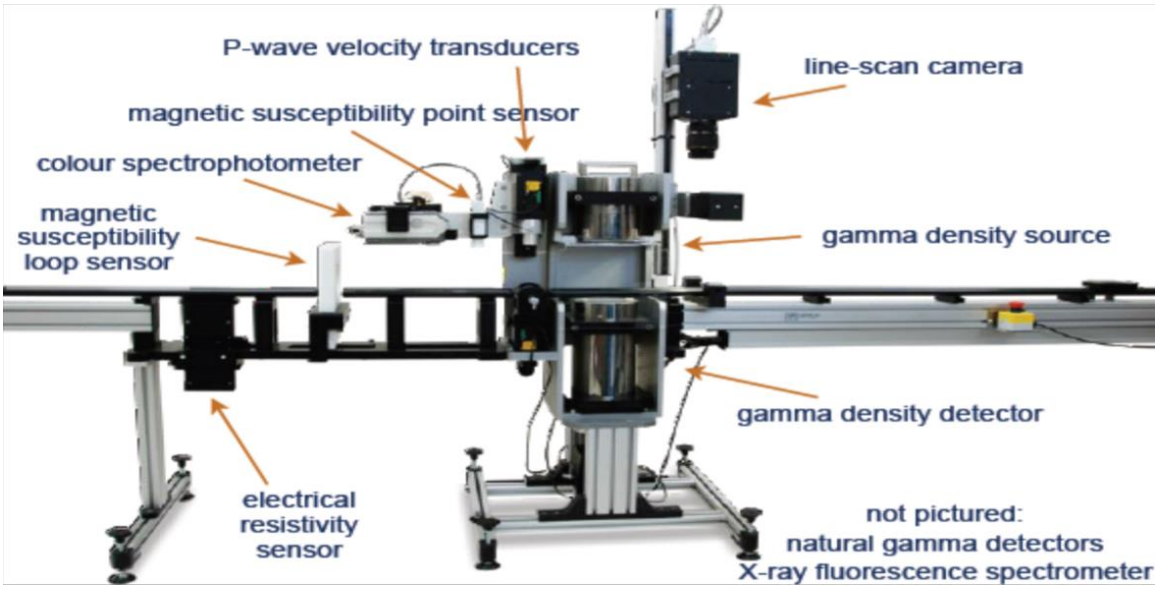

Figure 6. Representation of generalized MSCL system with attachments. From Geotek Ltd., Geotek Multi-Sensor Core Logger Flyer, Daventry, UK (2009).

susceptibility, and X-ray fluorescence (XRF). The accompanying Geotek software can measure travel time with a resolution of 1.5 m/s. The MSCL generated 11 MB of data in spreadsheet format and were named by their respective depths.

Plug Sampling

Once photography, medical CT scans, and MSCL concluded, the core was briefly analyzed for optimal depths to sample plugs. Plug samples were necessary because analyses on forthcoming CT scans and geomechanical testing required dimensions no larger than 1-inch diameter by 2-inch length. A couple of criteria were used to guide the sampling of plugs. The first consideration was the competency of core. It would be difficult to extract a plug from a highly fractured portion of soft rock as it would likely disintegrate during sampling, rendering future analysis impossible. Instead, competent, non-fractured sections of core were sought out. Given the age of the COST GE-1 core, much of it had already been reduced to rubble or oversampled from previous plug extraction. Visually, and with the help of medical CT results, sections of competent core were sought out and identified. Another criterion for sampling included visualizing the predominant lithology within the depth interval to identify representative plugs. Ultimately, seven plugs (Table 4) were sampled from the depth intervals listed in Table 3 using a high-pressure waterjet sub-coring machine.

Depth Interval (ft)	Depth of Extracted Core Plug (ft)
6607-6614	6608.5
6647.5-6655.4	6654
7040-7048	7046
7091-7098.9	7096.9
8352-8361	8360.5
9453-9460.9	9456.4
9501.8-9506.1	-
10545.9-10551	10550

Table 4. Plug depths (right) sampled from the depth interval loaned from DGS (left).

Industrial Computed Tomography

Once plugs were extracted, all seven samples were scanned by a North-Star Imaging Inc. M-5000® Industrial Computed Tomography System, seen in Figure 7. No sample preparation was necessary for this non-destructive analysis. Although a timely process that required a minimum of 90 minutes per scan, the industrial CT scanner produced higher resolution images than the medical CT scanner, ranging from 30-42 µm per pixel (NETL, 2017). Each image is a horizontal slice of the plug; when stacked, these individual images create a 3-dimensional (3D) representation of the core plug. This allowed for visualization, isolation, and quantification of interconnected porosity and fracture networks within rock. Overall, the industrial CT scanner produced 152 GB of TIFs.

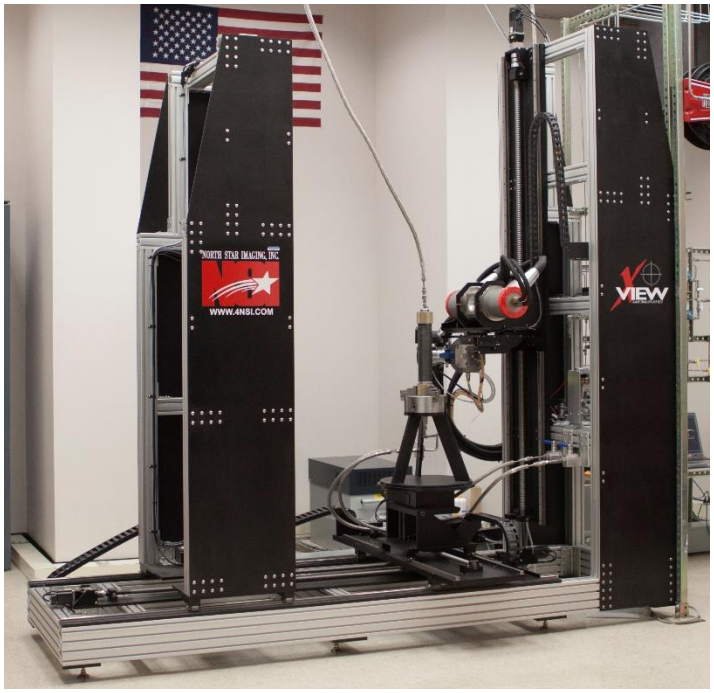

Figure 7. Image of the industrial CT scanner utilized onsite at NETL-MGN. From National Energy Technology Laboratory Flickr profile (2011).

Porosity Tests

Following industrial scans, all seven plug samples were transported to NETL-PGH to begin dynamic testing for rock properties and geomechanical parameters. Prior to testing for porosity, all plug samples were placed in a vacuum desiccator at 9% humidity for an hour to rid the samples of any moisture content. Then, each sample was subtly trimmed at each end to ensure a level surface and proper coupling with the core holder during geomechanical testing. Subsequently, each sample was measured for its diameter, length, and mass. After sample preparation, each plug was tested for its porosity using a TEMCO Helium Porosimeter HP-401, and dimensions and mass were input into LabVIEW based software. Three porosity tests were conducted, and the average was taken. From this, grain density and pore volume were also calculated. Outputs were in spreadsheet format.

Permeability Tests

After porosity tests, each plug sample was returned to the vacuum desiccator for an hour. Subsequently, each sample was tested for permeability in either a TEMCO UltraPerm-500 (N_2) Permeameter or a TEMCO Pulse-Decay Permeameter (PDP), but not both. The PDP is best used for ultra-low permeability rock (10 nD – 1 mD) in determination of caprock or tight gas sandstone. It sets a pore pressure throughout the plug, sends a differential pulse through the entire sample, and measures travel time to calculate permeability. The N_2 permeameter is a nitrogen flow-through tool best suited for moderate to high permeability samples (>1 mD). Permeability (*K*) is calculated using Darcy's Law (Equation 3):

$$K = \frac{Qnl}{S\Delta p} \quad \text{(Eqn. 3)}$$

where *n* is nitrogen viscosity at atmospheric conditions, *l* is the length of the sample, and *S* is cross-sectional area of the sample. Both permeameters held confining pressure constant with the

confining liquid as oil. The confining pressure varied between 1200-2000 pounds per square inch (psi) for the N_2 permeameter, and 1800 psi for the PDP. Outputs were in spreadsheet format.

Dynamic Geomechanical Tests

Once permeability tests concluded, each plug was placed in New England Research Group (NER) AutoLab 1500 device. This device is capable of triaxial compression, allows the user to adjust confining, pore, and effective pressure, and contains ultrasonic wave transducers which generate compressional and shear waves on one end of the sample and record the arrival on the other end. It can also record physical characteristics such as Young's modulus (E) and Poisson's ratio (ν). These values are calculated using Equations 4 and 5, respectively, in terms of compressional wave (V_P) and shear wave (V_S) velocities where ρ = bulk density (Murayama et al., 2013):

$$E = \frac{\rho {V_S}^2 (3{V_P}^2 - 4{V_S}^2)}{{V_P}^2 - {V_S}^2} \quad \text{(Eqn. 4)}$$

$$\nu = \frac{1 - 2(\frac{V_S}{V_P})^2}{2(1 - \left(\frac{V_S}{V_P}\right)^2)} \quad \text{(Eqn. 5)}$$

Additionally, shear modulus (μ), bulk modulus (K), and Lame's first parameter (λ) were calculated using Equations 6, 7, and 8, respectively (De Beer and Maina, 2008):

$$\mu = \frac{E}{2 + 2\nu} \quad \text{(Eqn. 6)}$$

$$K = \frac{E}{3(1 - 2\nu)} \text{ (Eqn. 7)}$$

$$\lambda = \frac{E\nu}{(1 + \nu)(1 - 2\nu)} \text{ (Eqn. 8)}$$

For this study, only uniaxial compression testing was conducted and pore pressure was kept constant due to time constraints. All samples experienced two confining pressure cycles (ramped

up, down, up, then down) from 12-52 Megapascals (MPa). Measurements for travel time, Young's modulus, and Poisson's ratio were taken at 4 MPa steps. Outputs from the AutoLab 1500 were compiled in tables in PDF format.

Upon completion of dynamic geomechanical testing, all COST GE-1 drill core and extracted plug samples were returned to DGS along with a copy of all derivative data. A summary of data generated for each phase of testing can be seen in Table 5. Upon completion of this study, all data was publicly released on NETL's Energy Data eXchange (EDX).

Experiment	Date Generated On:	Data Volume	Attainable Rock Properties
Core Photographs	Slabbed Core	238 MB	
Medical CT scans	Slabbed Core	14 GB	Bulk density
MSCL	Slabbed Core	11 MB	XRF, gamma density
Industrial CT Scans	Plug	152 GB	Fractures, effective porosity, mineralogy
Permeability Tests	Plug	155 KB	Permeability
Porosity Tests	Plug	19 KB	Porosity
Dynamic Mechanical Tests	Plug	8 MB	In-situ P-wave, S-wave, Young's modulus, Poisson's ratio

Table 5. A summary of all data generated, including volume of data and attainable rock properties.

CHAPTER IV

DATA ANALYSIS & RESULTS

A large volume of data was generated during this study, and not all of it fits within the context of the research objectives. It was not essential to comprehensively analyze all data; certain datasets were given higher priority for analysis than others. For example, MSCL data detailing XRF, gamma density, and magnetic susceptibility information were excluded from analysis. However, this presents an opportunity for future SE-ACM and COST GE-1 research.

Medical CT Results

Medical CT scans were primarily utilized for locating proper plug sampling depths. However, TIF images generated from CT allow for a bulk 3D volumetric characterization of core and complement MSCL data if they are processed and combined into TIF stacks. Medical CT scans generate images in greyscale colored by CT number. CT number is directly proportional to variations in attenuation, and therefore indicative of relative density within the rock (Tanaka, 2011; NETL, 2017). Dark sections are less dense than bright sections. To test this, depth-aligned 2D cross sections through the middle of the core were integrated into Petrel for a visual comparison with wireline bulk density (RHOB) logs. A general positive trend was revealed. An example can be seen in the left image in Figure 8. Darker (lower CT) sections of core correspond to lower RHOB values in wireline. In addition, fractures and bedding structures can be discriminated within COST GE-1 core, highlighting the heterogeneity in finer scale (< 1 ft)

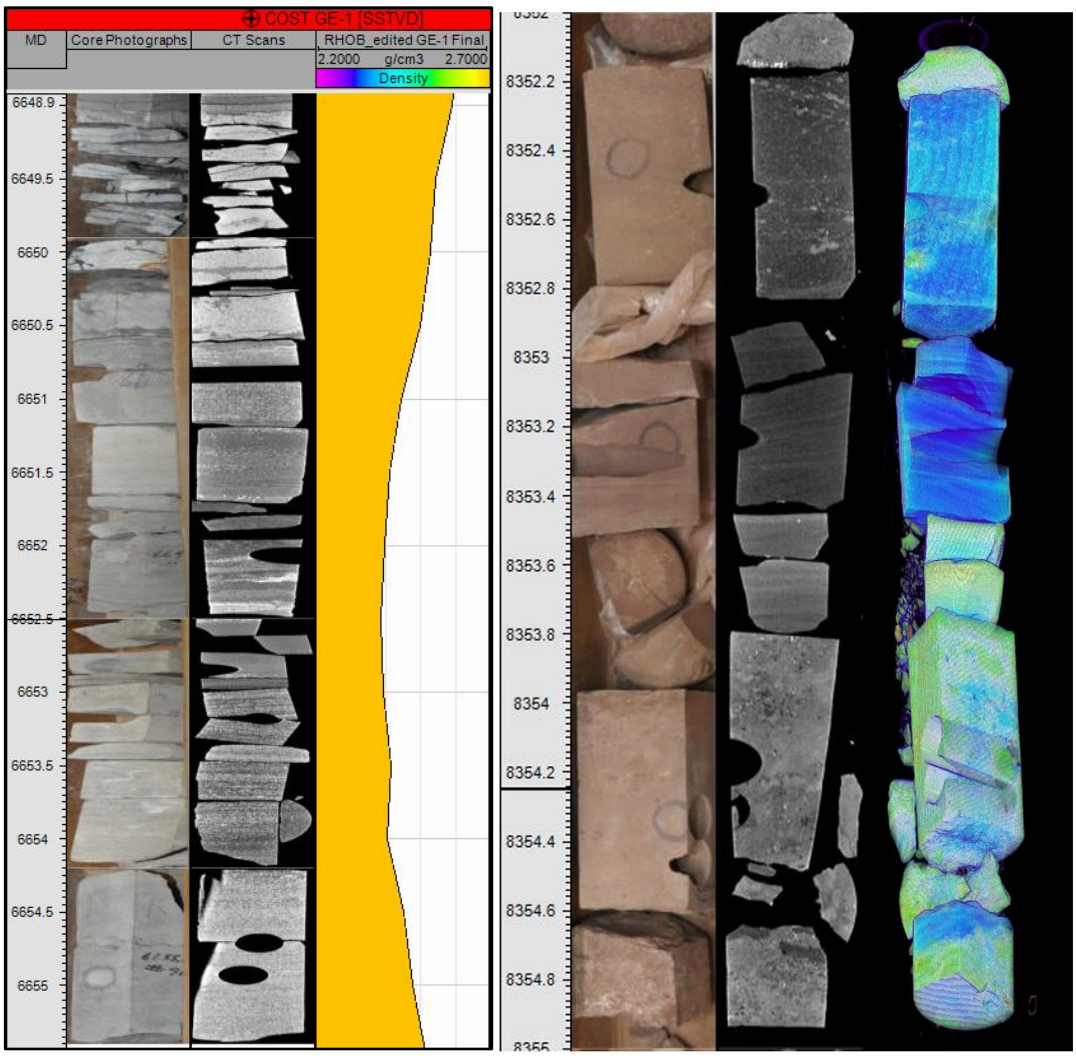

Figure 8. A comparison between core photography, medical CT cross-sectional slice, and (Left) wireline RHOB response for depth interval 6648.9-6655.5 ft., and (Right) Thermal LUT filter for depth interval 8352-8355 ft.

domain regimes not detectable by low-resolution RHOB. To study these domain regimes closer, a thermal Lookup Table (LUT) filter was applied to all TIF stacks using open-source image processing software ImageJ. A thermal LUT filter is a rendering option and plugin within ImageJ that color codes the gradation of image intensity to create a “heat map” ranging from blue (lowest relief) through green and yellow to red (highest relief). Simply put, this filter characterizes heterogeneity by highlighting fine-scale density variations. Depth-aligned, side-by-side

comparisons of all medical CT scan results with white light core photographs can be seen in Appendix B.

Porosity & Permeability

Porosity and permeability were measured for every plug sample and are shown in Table 6. The highest porosities and permeabilities were measured on plugs 7096.9 and 8360.5, reaching 21% porosity and 365 mD permeability. For those samples that registered higher permeabilities that could be targets for potential CO_2 reservoirs, the Klinkenberg permeability was calculated. Air permeability is always greater than the permeability attained when using a liquid as the flowing fluid. The Klinkenberg calculation corrects for gas slippage when using air as the flowing fluid in the case of the N_2 permeameter, and results in a measurement more indicative of liquid, such as supercritical CO_2.

Industrial CT Results

The same processing steps to create medical CT TIF stacks was applied to industrial CT images to create higher-resolution (30-42 µm per pixel) 3D volumetric representations of plugs. This new perspective provides an opportunity to examine minerals, large crystals, details of fractures, and discontinuities within the plug. For the purposes of this study, a methodology was created to quantify interconnected porosity in potential reservoir rock in ImageJ.

After loading the TIF stack of a plug sample in ImageJ, the first step necessary is to rid the stack of the most commonly encountered artifact in CT scanning: beam hardening. This is a result of attenuation of lower-energy X-rays creating a diminishing effect in overall CT intensity, creating a plug image that appears darker in the center and brighter along the edges (Park, 2015). This can be corrected for in different ways. The correction used in this study was Color Correction. This is a filter built-in to ImageJ that changes greyscale values by recognizing difference in color from edges to center, creating a color gradient, and then adding or subtracting

Core Plug (ft)	Mass (g)	Bulk Volume (cm^3)	Bulk Density (g/cm^3)	Porosity (%)	Pore Volume (cm^3)	Grain Volume (cm^3)	Grain Density (g/cm^3)	Permeability (mD)
6608.5	68.864	27.958	2.463123	9.7	2.701333	25.25667	2.726567	2.34
6654	72.237	28.693	2.517583	11.2	3.2	25.493	2.833601	0.048
7046	90.56	35.669	2.538899	6.3	2.23	33.439	2.708215	0.022
7096.9	62.531	31.319	1.996584	21.3	6.668	24.651	2.536652	223
8360.5	60.985	28.488	2.140726	17.5	4.976	23.512	2.593782	351.12
9456.4	75.391	28.292	2.664746	4.9	1.3944	26.8976	2.802889	0.003
10550	63.773	27.807	2.293415	11.3	3.1308	24.6762	2.584393	5.970

Table 6. Porosity and permeability results as well as dimensions for each plug.

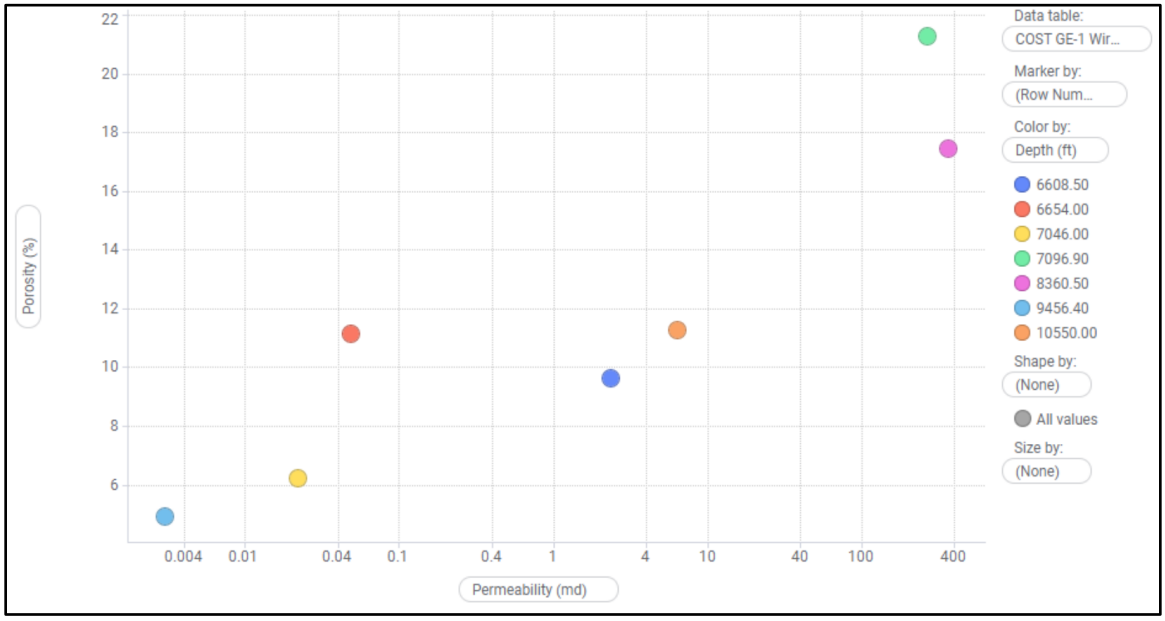

Figure 9. Porosity and permeability crossplot displaying results from each plug, colored by depth. Permeability is displayed on a logarithmic scale.

those values from greyscale values. A before-and-after example can be seen in Figure 10. Following color correction, a histogram of greyscale values was compiled for every image in the TIF stack. The next steps that follow were iterative through trial and error until the percentage of selected volume matched the pore volume values calculated from porosity tests for that specific plug sample:

1. Created a threshold by selecting a portion of lower values in the greyscale histogram
2. Isolated selected volume.
3. Converted image to a binary image. This reduces the image to two values: black (background) and white (selected volume).
4. Used Voxel Counter to measure total selected volume.

These steps are visualized in Figure 11 and were repeated until the selected volume matched pore volume values calculated in the porosimeter. The BoneJ plugin called Purify was then utilized to quantify percentage of interconnected volume within the pore volume, as seen in the bottom right image of Figure 11. This methodology was only conducted on the two high-porosity plug samples: 7096.9 and 8360.5. Calculated interconnected porosities are seen in Table 7.

Similar to the medical CT scans, thermal LUT filter was also applied to industrial CT scans to help highlight "hotspots", or high-density features, within each plug sample. Along with grayscale 3D representations, these can be found in Appendix C.

Core Plug (ft)	Porosity - Porosimeter (%)	Pore Volume - Porosimeter (cm^3)	Volume of Stack (cm^3)	Thresholded Volume (cm^3)	Interconnected Porosity (%)
7096.9	21.29	6.668	24.154	22.581	16.23
8360.5	17.47	4.976	24.715	23.519	15.84

Table 7. Core plugs 7096.9 and 8360.5 and their calculated interconnected porosities.

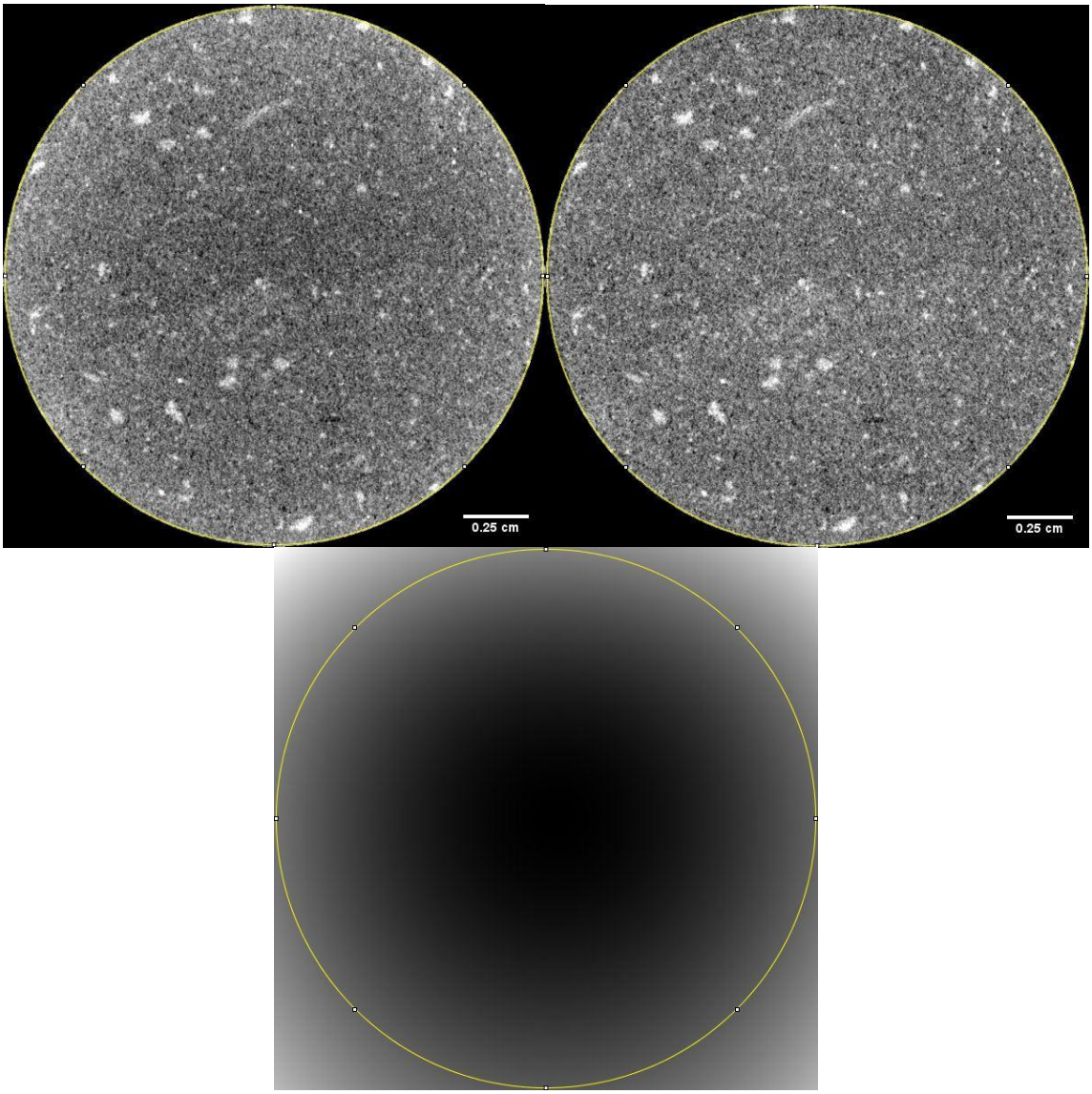

Figure 10. Applying a color correction filter to plug 7096.9. [Top Left] Pre-filtered image with noticeable bright edges and darkened center. [Top Right] Post-filtered image with even color distribution. [Bottom] Applied color gradient filter.

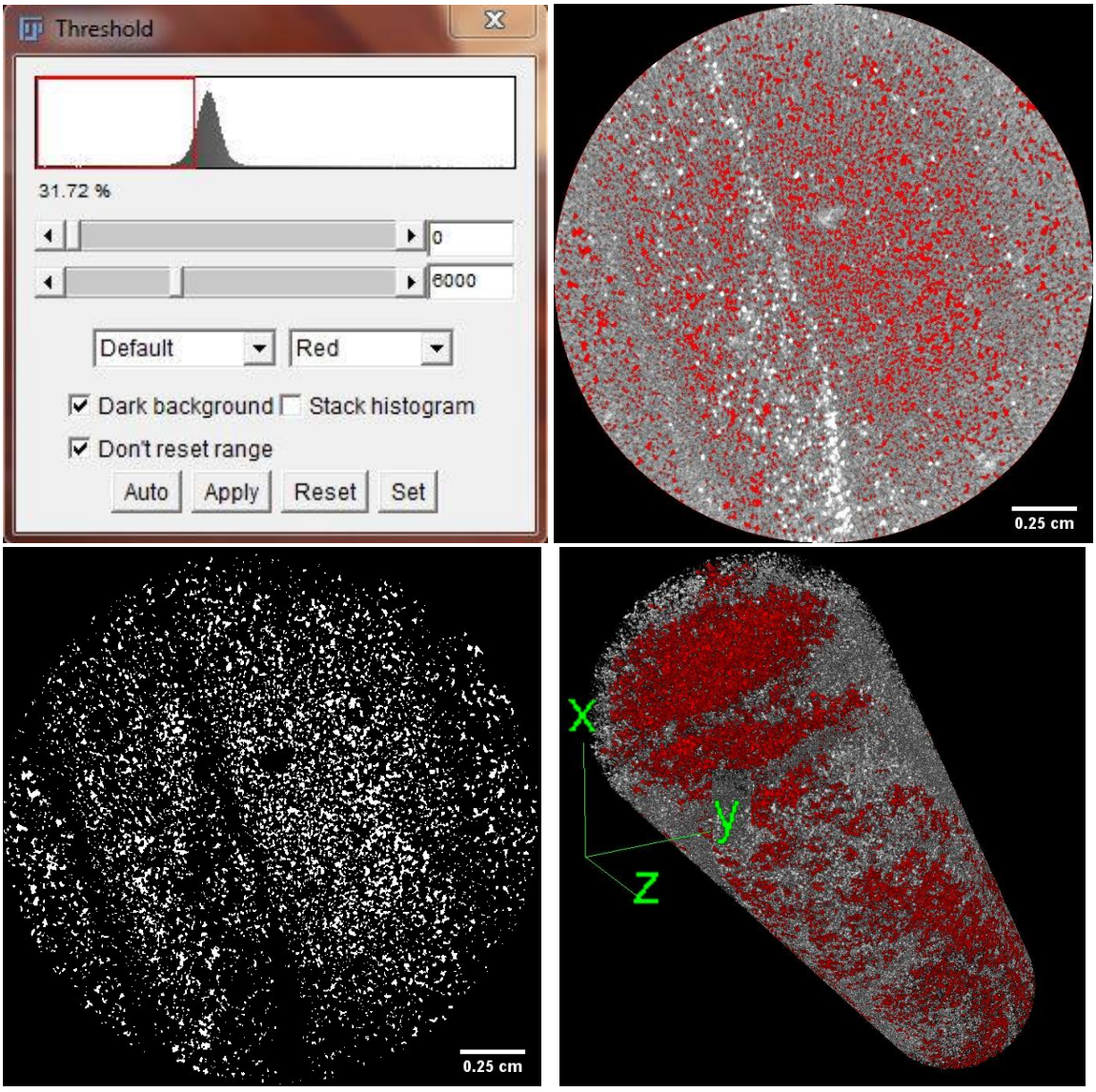

Figure 11. Identifying interconnected volume within plug 8360.5. [Top Left] Selecting the bottom 31.72% of greyscale values within the TIF stack. [Top Right] Selected percentage shown in red. [Bottom Left] Binary image of selected percentage in white. Voxel Counter calculated selected area throughout the stack to calculate selected volume, which matched pore volume. [Bottom Right] Interconnected volume shown in red against isolated volume in gray.

Dynamic Geomechanical Results

Results from the AutoLab 1500 dynamic tests reveal the relationship between changes in effective pressure and in-situ rock properties in proposed intervals for reservoirs and seals. Although all samples survived mechanical testing intact, two samples encountered problems that should be noted during analysis. Sample 7046 was spoiled with oil during mechanical testing but can be analyzed as a core sample partially saturated with hydrocarbons. Sample 7096.9 experienced a power outage during the second pressure ramp, which limited data return.

Plots of effective pressure change with Young's modulus (Figure 12) display two noticeable clusters of data. One cluster of samples is centered around 40-50 GPa indicating stiffer rock, and the other is clustered between 15-30 GPa indicating less stiff rock. One intriguing sample, 9456.4, appears to span the area between these clusters. Upon further examination in crossplot of Young's modulus with Poisson's ratio, 9456.4 appears anomalous with negative Poisson's ratio values as seen in Figure 13. Although an unusual result, a negative Poisson's ratio could indicate a couple of things.

Poisson's ratio is a constant that describes the elasticity of a rock and its significance is underrated (Gercek, 2007). Commonly, materials expand laterally when stretched creating longitudinal extensional strain in the direction of the stretching force. Virtually all materials become narrow in cross section when stretched, resulting in a positive Poisson's ratio. If a material expands laterally when stretched, it has a negative Poisson's ratio (Huang, 2016) and is classified as an *auxetic* rock (Gercek, 2007). Although this is considered rare in nature, Zaitsev et al. (2017) studied q-ratios of 90 rock samples with a high abundance of cracks and discovered a significant number of samples with negative Poisson's ratio. Their results showed that samples

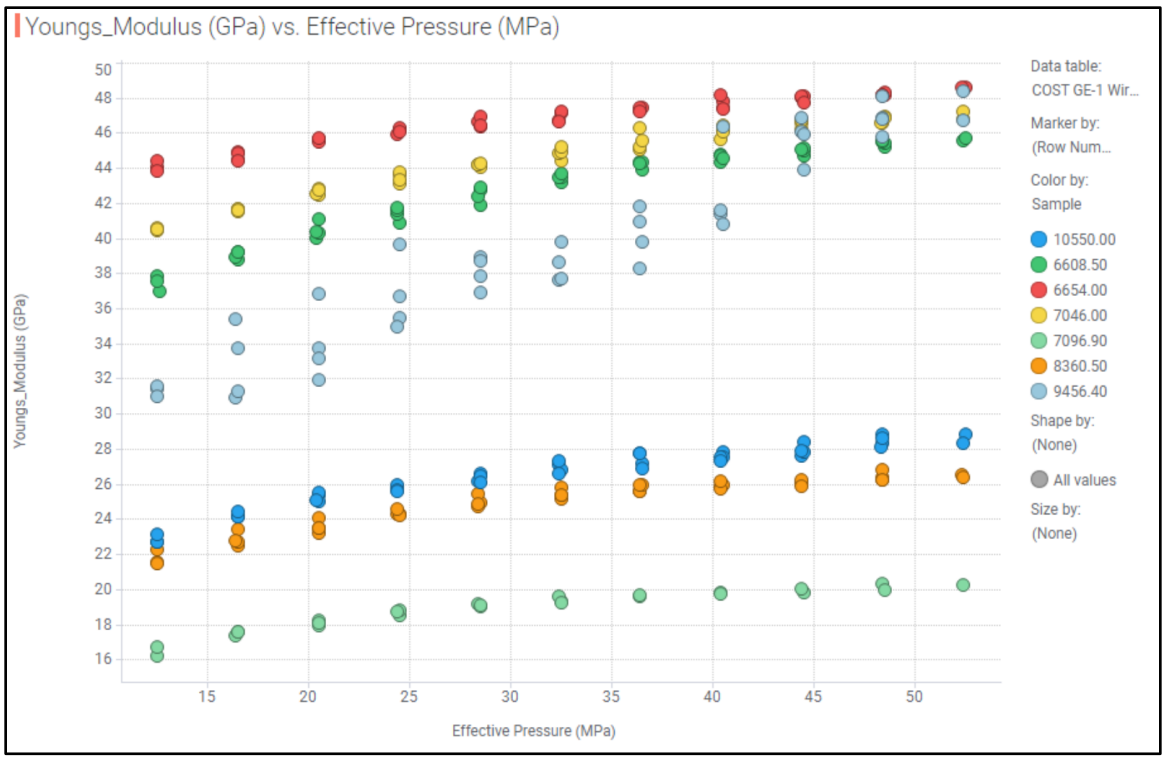

Figure 12. A crossplot of Young's modulus and effective pressure.

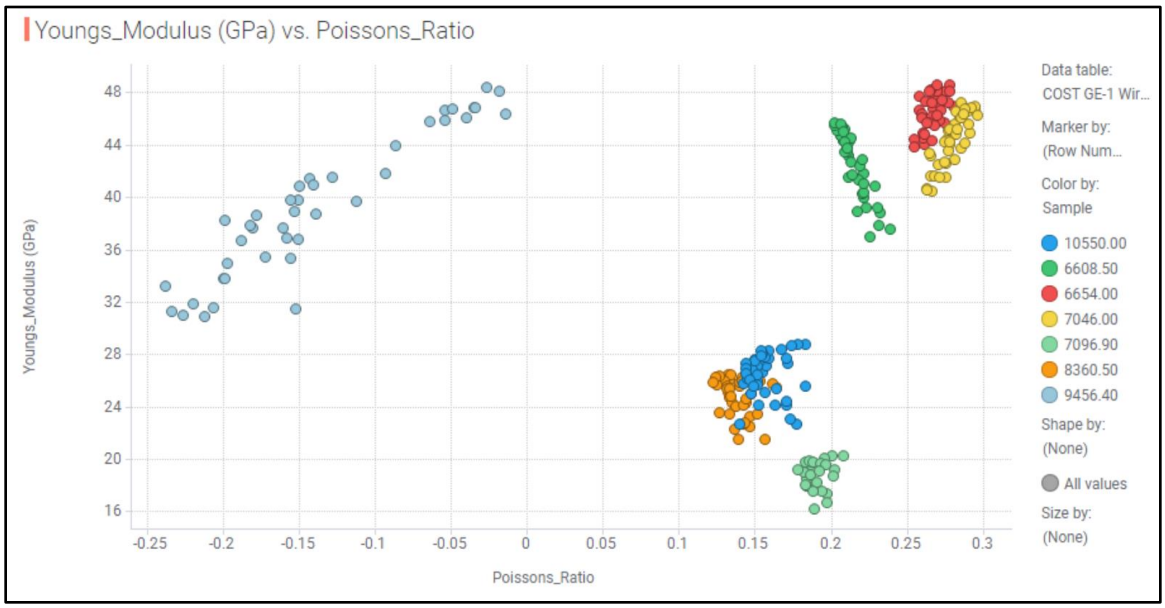

Figure 13. A crossplot of Young's modulus and Poisson's ratio displaying an intriguing value for sample 9456.4.

with smaller ratios of normal compliance cracks to shear cracks return positive Poisson's ratios, while higher ratios of normal compliance cracks to shear cracks result in negative Poisson's ratios. This contrasts with the convention that these occurrences are exotic in nature (Zaitsev et al., 2017). This finding agrees with theoretical models for granular materials and cracked solids where negative Poisson's ratio can be observed in nearly isotropic material with distorted normal compliances (Zaitsev and Sas, 2000; Pasternak and Dyskin, 2012).

Another possible cause of negative Poisson's ratio in sample 9456.4 is instrument error. All samples were mechanically tested on the same equipment with the same sample preparation and input parameters and operated by the same researcher. The sample did not had no indications of deformation or spoilage following testing. According to the equipment operator, the issue could not be explained but was assumed to be an issue with the AutoLab software program. Poisson's ratio values for this sample should be analyzed "with some skepticism" (Spaulding, 2019). No other sample exhibited a comparable issue, although this was the final sample mechanically tested.

CHAPTER V

DISCUSSION & IMPACT OF RESULTS

Constraining CO_2 Storage Capacity

In absence of specific geologic variables or areas of uncertainty in geologic properties, ranges can be used to estimate the three geologic efficiency factors in Equation 2. However, where they are known, they should be implemented in the calculation (IEA GHG, 2009). With the help of CT image analysis, this study presented a workflow to quantify interconnected porosity for two potential shallow shelf clastic reservoirs for CO_2 storage. These values can be used as close substitutes for effective porosity to further constrain the range of possible values and reduce uncertainty. For shallow shelf clastic depositional environments, IEA GHG (2009) presents a range of 0.62-0.78 for E_φ. Using the values listed in Table 7, this study arrived at an E_φ= 0.83. This value, which is slightly above the range given by IEA GHG, should be considered an overestimate since these are interconnected porosity values that do not account for fluid flow.

Another variable that requires updating within the CO_2 storage calculation in Equation 1 is gross thickness of reservoir (h_g). Among the recommended reservoir intervals in the Lower Cretaceous and Upper Jurassic sections, two out of four core samples met the storage criteria of porosity (>20%) and permeability (>200 mD) for the SE-ACM region (see Table 8) (Almutairi, 2018). The other two samples illuminated the heterogeneity within the Lower Cretaceous and Upper Jurassic intervals with tight sandstone and impermeable carbonate lithologies.

Core Plug (ft)	Proposed	Porosity (%)	Permeability (mD)
6608.5	Seal	9.7	2.34
6654	Seal	11.2	0.048
7046	Reservoir	6.3	0.022
7096.9	Reservoir	21.3	223
8360.5	Seal/Reservoir	17.5	351.12
9456.4	Reservoir	4.9	0.003
10550	Seal	11.3	5.970

Table 8. Each plug sample and its proposed seal or reservoir interval. Green rows indicate that porosity and permeability values match storage criteria. Red rows indicate no match. Sample 8360.5 was proposed as both seal and reservoir (Almayahi, in prep).

Seal Integrity

Integrity of a proposed seal refers to geomechanical properties of the caprock and evaluates the caprock for the likelihood of developing structural permeability from creating new or reactivating old fractures. Factors that influence this include lithology, stress fields, and stress changes caused by injection (IEA GHG, 2011). The International Energy Agency Greenhouse Gas (IEA GHG) program recommends calibrating potential seals using Integrity Factor (1.0 - 0) from the upper left of Figure 14 to the bottom right. This grades each lithology on the propensity to develop structural permeability using compressibility and strength on the x-axis, and velocity and ductility on the y-axis. With velocity and compressibility information generated during this study combined with lithology information (Scholle, 1979) for four proposed seal intervals (see Table 8), each seal sample was plotted on Figure 14. Although their velocities vary significantly, their lithologies are very similar with three samples defined as carbonate rock. Limestone and calcareous shale are not ideal caprocks due to their brittleness and propensity to fracture. Overall, all four classify with Integrity Factor scores below 0.5.

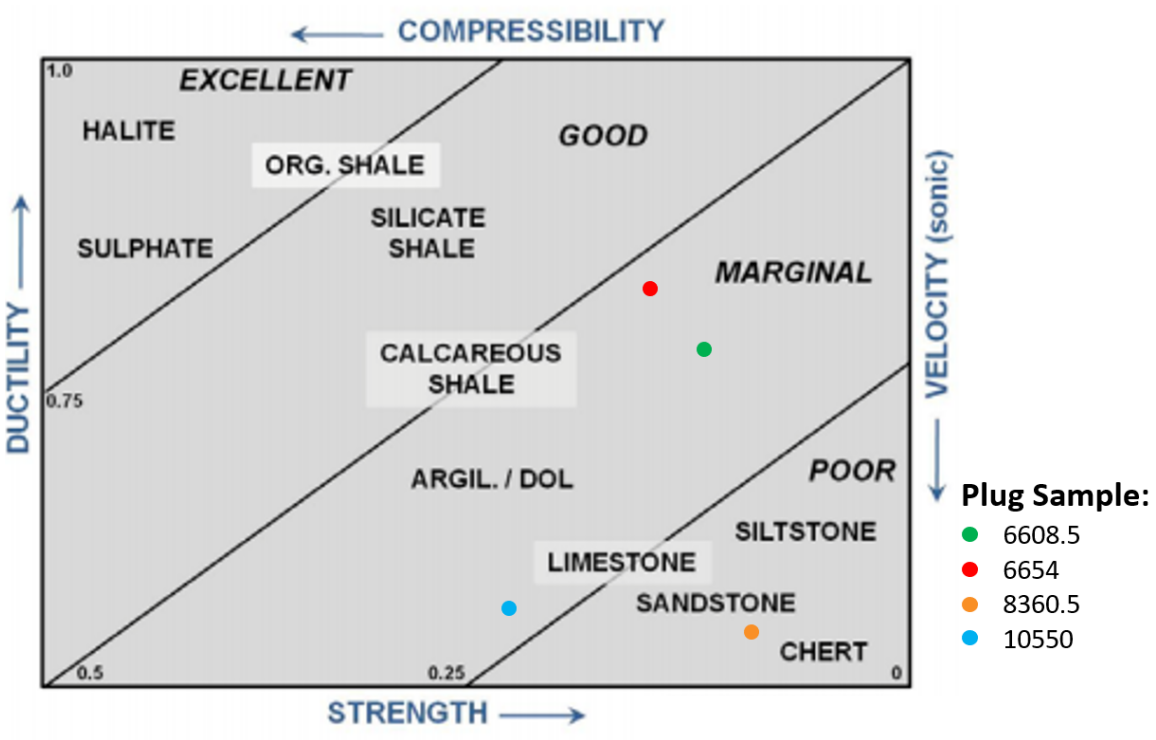

Figure 14. A plot of the four proposed seal samples based on velocity and lithology.

Caveats & Recommendations

Prospecting for CO_2 storage potential in the SE-ACM comes with many drawbacks. A comprehensive and accurate assessment of CO_2 capacity is difficult given the lack of subsurface data in the region. Previous studies noted the lack of 3D seismic data needed to fill in areas of uncertainty between 2D seismic lines (Almutairi, 2018; Ollmann, 2018). Lateral continuity of reservoir and seal horizons are assumed given the passive margin history. However, without 3D seismic data, this cannot be confirmed. With only one cored well in the study area, it is difficult to ground-truth seismic analyses. This study would have benefited from greater access to drill core. Reservoirs and seals intervals proposed by Almutairi (2018) do not have existing core, so 32 Gt of potential storage in the Upper Cretaceous had to be excluded from this study. Another disadvantage for CO_2 storage prospectivity in the SE-ACM is the lack of proven permanence.

Because there have been no hydrocarbon discoveries in the region, there is no evidence that the proposed seal intervals can entrap and store CO_2 long-term.

There are several next steps that are recommended going forward to accurately assess CO_2 storage potential in the SE-ACM. Above all others, this 11,000 mi^2 region would greatly benefit from a 3D seismic survey around the high-density data coverage in the Southeast Georgia Embayment. To help ground-truth new and existing surveys, it is also recommended to drill and core a deep well to better understand lithologic heterogeneity across the region. Furthermore, once this core is acquired, it would be advantageous to conduct CO_2 flow-through experiments and SEM analysis to gather information on effective porosity and CO_2 geochemical interactions.

CHAPTER VI

CONCLUSIONS

The SE-ACM region has immense capacity for CO_2 storage with upwards of 32 Gt in the Upper Cretaceous (Almutairi, 2018; Ollmann, 2018) and likely more in the Lower Cretaceous and Upper Jurassic (Almayahi, *in prep*). This study helped to ground-truth previous seismic-focused assessments using the only drill core available in the area: COST GE-1.

From this drill core, it was possible to generate a wealth of data that provide a better understanding of the geologic picture beneath the SE-ACM. An optimized workflow was designed around the remaining COST GE-1 core and stipulations set by DGS to maximize data generation while also minimizing destructive analyses. Cutting-edge equipment that fits this scope was selected at DOE's NETL including a multi-sensor core logger and two CT scanners capable of generating high-resolution TIF images interpretable for bulk density and interconnected porosity. Following specific depth interval selection for plug sampling, porosity and permeability were measured. Each plug underwent dynamic mechanical testing to extract critical geomechanical parameters that provide a better understanding of how the rock responds to changes in effective pressure.

Analysis began by comparing CT number in medical CT scans to wireline RHOB values and identified a positive trend. Porosity and permeability results were compiled, and their relationship was displayed in crossplot. Subsequently, porosity values were used to develop an

analysis workflow to quantify interconnected porosity within plug samples using 3D industrial CT images. Finally, mechanical testing generated velocities and elastic moduli to help characterize an anomalous auxetic rock. With these analyses, reservoir-specific interconnected porosity values were used to refine and constrain a CO_2 efficiency factor. It was also recommended to revisit calculations for reservoir thickness across the SE-ACM due to apparent heterogeneity in many proposed reservoir intervals. Using velocities and lithological knowledge, seal integrity was plotted for four proposed seal intervals.

The SE-ACM has great potential for CO_2 storage, but currently lacks sufficient data coverage to make accurate assessments of storage volume, lateral continuity of seals and reservoirs, and permanence. However, it would greatly benefit geologic knowledge and history of the Atlantic Continental Margin if a 3D seismic survey was acquired and a pilot hole was drilled.

REFERENCES

Almayahi, D. "Evaluation of CO2 Storage Potential in Offshore Lower Cretaceous Strata in mid-South Atlantic Ocean, Southeast United States." Masters Thesis. Oklahoma State University, Stillwater, Oklahoma, *in prep*.

Almutairi, Khaled F. "Assessment Of Upper Cretaceous Strata For Offshore CO2 Storage: Southeastern United States," PhD Dissertation, University of South Carolina, Columbia, South Carolina, 2018. 107.

Beck, Lee. "Carbon Capture and Storage in the USA: The Role of US Innovation Leadership in Climate-Technology Commercialization." *Clean Energy* 4, no. 1 (April 4, 2020): 2–11. https://doi.org/10.1093/ce/zkz031.

Dillon, William P, Charles K Paull, Richard T Buffler, and Jean-Pierre Fail. "Structure and Development of the Southeast Georgia Embayment and Northern Blake Plateau: Preliminary Analysis," (July 20, 1977): 15.

Dillon, William P., and Peter Popenoe. "The Blake Plateau Basin and Carolina Trough." In *The Atlantic Continental Margin*, edited by Robert E. Sheridan and John A. Grow, 291–328. Londan: Geological Society of America, 1988. https://doi.org/10.1130/DNAG-GNA-I2.291.

DOE. "Internal Revenue Code Tax Fact Sheet." United States Department of Energy, Fossil Energy, accessed 20 June 2019. <https://www.energy.gov/sites/prod/files/2019/10/f67/Internal%20Revenue%20Code%20Tax%20Fact%20Sheet.pdf>

EPA. "Sources of Greenhouse Emissions." United States Environmental Protection Agency, accessed 20 June 2019. < https://www.epa.gov/ghgemissions/sources-greenhouse-gas-emissions>

Fukai, Isis, Laura Keister, Priya Ravi Ganesh, Lydia Cumming, Will Fortin, and Neeraj Gupta. "Carbon Dioxide Storage Resource Assessment of Cretaceous- and Jurassic-Age Sandstones in the Atlantic Offshore Region of the Northeastern United States." *Environmental Geosciences* 27, no. 1 (March 2020): 25–47. https://doi.org/10.1306/eg.09261919016.

Gercek, H. “Poisson’s Ratio Values for Rocks.” *International Journal of Rock Mechanics and Mining Sciences* 44, no. 1 (January 2007): 1–13. https://doi.org/10.1016/j.ijrmms.2006.04.011.

Goodman, Angela, Sean Sanguinito, and Jonathan S. Levine. “Prospective CO2 Saline Resource Estimation Methodology: Refinement of Existing US-DOE-NETL Methods Based on Data Availability.” International Journal of Greenhouse Gas Control 54 (November 2016): 242–49. https://doi.org/10.1016/j.ijggc.2016.09.009.

Hills, Denise J, and Jack C Pashin. “FINAL REPORT: Southeastern Regional Carbon Sequestration Partnership (SECARB) Phase III-Task 15: Preliminary Evaluation of Offshore Transport and Storage of CO2,” 2010. https://doi.org/10.13140/RG.2.2.33279.66721.

Huang, Chuanwei, and Lang Chen. “Negative Poisson’s Ratio in Modern Functional Materials.” *Advanced Materials* 28, no. 37 (October 2016): 8079–96. https://doi.org/10.1002/adma.201601363.

IEA Greenhouse Gas R&D Programme (IEA GHG). “Development of Storage Coefficients for CO2 Storage in Deep Saline Formations.” (October 13, 2009).

IEA Greenhouse Gas R&D Programme (IEA GHG)., “Caprock Systems for CO2 Geological Storage”. (June 1, 2011).

Kovscek, A. R. “Screening Criteria For CO2 Storage in Oil Reservoirs.” *Petroleum Science and Technology* 20, no. 7–8 (January 7, 2002): 841–66. https://doi.org/10.1081/LFT-120003717.

Midldeton, Richard S., Jonathan S. Levine, Jeffrey M. Bielicki, and Philip H. Stauffer. “Industrial CO2 and Carbon Capture: Near-Term Benefit, Long-Term Necessity.” *Energy Procedia* 114 (July 2017): 7601–5. https://doi.org/10.1016/j.egypro.2017.03.1892.

Mitchell, Kenneth L. “Mitigation of Greenhouse Gases in the Southeast USA.” In *Climate of the Southeast United States*, edited by Keith T. Ingram, Kirstin Dow, Lynne Carter, and Julie Anderson, 271–94. Washington, DC: Island Press/Center for Resource Economics, 2013. https://doi.org/10.5822/978-1-61091-509-0_12.

NETL. “Best Practices: Site Screening, Site Selection, and Site Characterization for Geologic Storage Projects.” 2017 edition. (June 2017).

NETL. “Characterization of the Martinsburg Formation using Computed Tomography and Geophysical Logging Techniques.” *NETL-TRS-4-2017*. (March 2, 2017).

Ollmann, John. “Velocity Model for CO2 Sequestration in the Atlantic Continental Margin.” Masters Thesis, University of South Carolina, Columbia, South Carolina, 2018.

Park, Hyoung Suk, Yong Eun Chung, and Jin Keun Seo. "Computed Tomographic Beam-Hardening Artefacts: Mathematical Characterization and Analysis." *Philosophical Transactions of the Royal Society A: Mathematical, Physical and Engineering Sciences* 373, no. 2043 (June 13, 2015): 20140388. https://doi.org/10.1098/rsta.2014.0388.

Pasternak, E., and A.V. Dyskin. "Materials and Structures with Macroscopic Negative Poisson's Ratio." *International Journal of Engineering Science* 52 (March 2012): 103–14. https://doi.org/10.1016/j.ijengsci.2011.11.006.

Pinet, Paul R, and Peter Popenoe. "Shallow Seismic Stratigraphy and Post-Albian Geologic History of the Northern and Central Blake Plateau," n.d., 12.

Pogge von Strandmann, Philip A. E., Kevin W. Burton, Sandra O. Snæbjörnsdóttir, Bergur Sigfússon, Edda S. Aradóttir, Ingvi Gunnarsson, Helgi A. Alfredsson, Kiflom G. Mesfin, Eric H. Oelkers, and Sigurður R. Gislason. "Rapid CO2 Mineralisation into Calcite at the CarbFix Storage Site Quantified Using Calcium Isotopes." *Nature Communications* 10, no. 1 (December 2019): 1983. https://doi.org/10.1038/s41467-019-10003-8.

Maher, John C. "Geologic Framework and Petroleum Potential of the Atlantic Coastal Plain and Continental Shelf." United States Geological Survey Professional Paper. (1971).

Scholle, Peter A. "Geological Studies of the COST GE-1 Well, United States South Atlantic Outer Continental Shelf Area." *Geological Survey Circular 800*. (1979).

Schrag, D. P. "Storage of Carbon Dioxide in Offshore Sediments." *Science* 325, no. 5948 (September 25, 2009): 1658–59. https://doi.org/10.1126/science.1175750.

Schutjens, Peter, and Wolfgang Heidug. "On the Pore Volume Compressibility and Its Application as a Petrophysical Parameter." 9th Biennial International Conference & Exposition on Petroleum Geophysics. N.d., 17.

Zaitsev, V. and Sas, P. "Elastic Moduli and Dissipative Properties of Microinhomogeneous Solids with Isotropically Oriented Defects." Acustica Vol. 86. (February 17, 2000): 216-228.

Zaitsev, Vladimir Y., Andrey V. Radostin, Elena Pasternak, and Arcady Dyskin. "Extracting Real-Crack Properties from Non-Linear Elastic Behaviour of Rocks: Abundance of Cracks with Dominating Normal Compliance and Rocks with Negative Poisson Ratios." *Nonlinear Processes in Geophysics* 24, no. 3 (September 5, 2017): 543–51. https://doi.org/10.5194/npg-24-543-2017.

APPENDICES

APPENDIX A

COST GE-1 Lithology Log

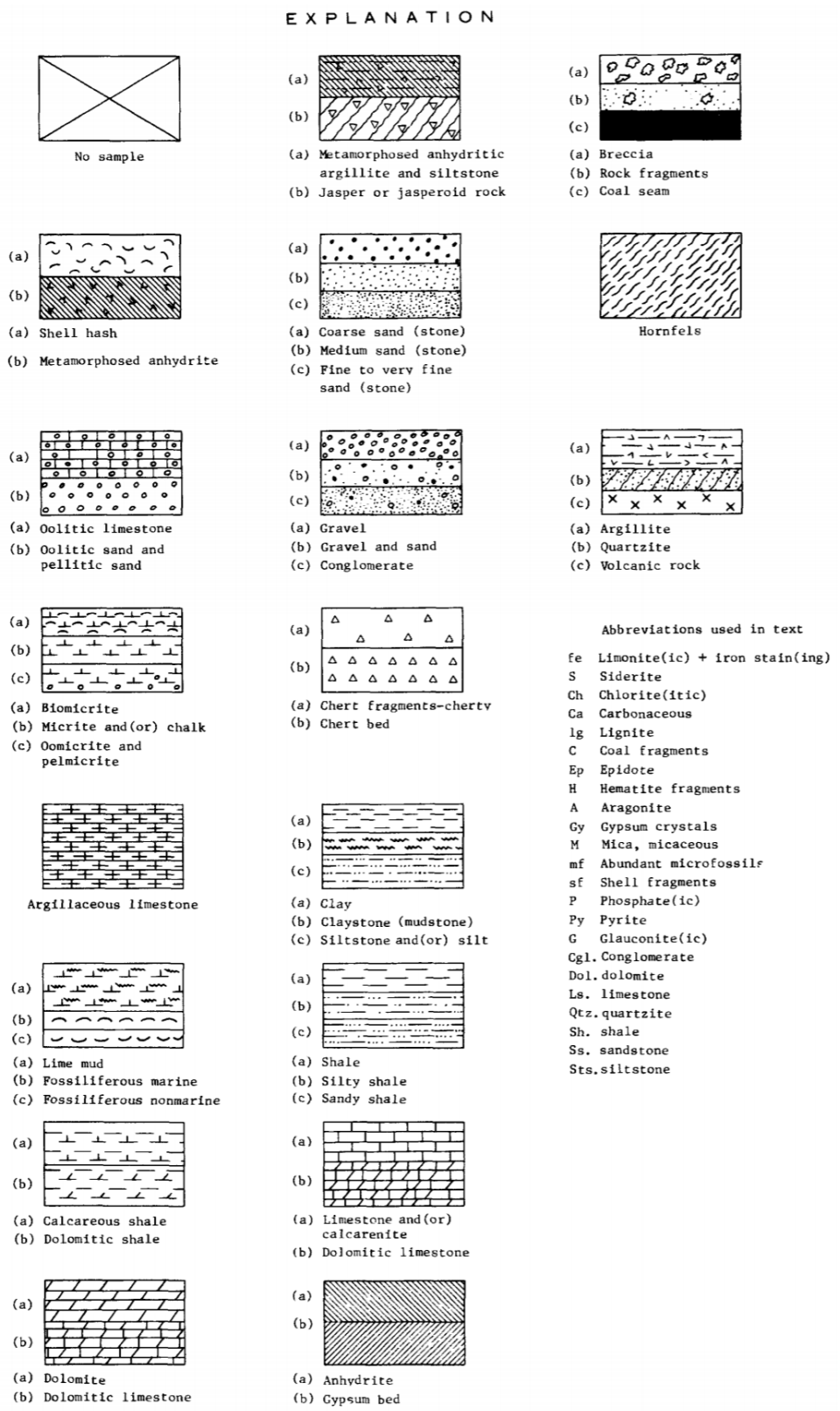

Figure A1: Legend for lithologic log, COST GE-1 Well (Scholle, 1979).

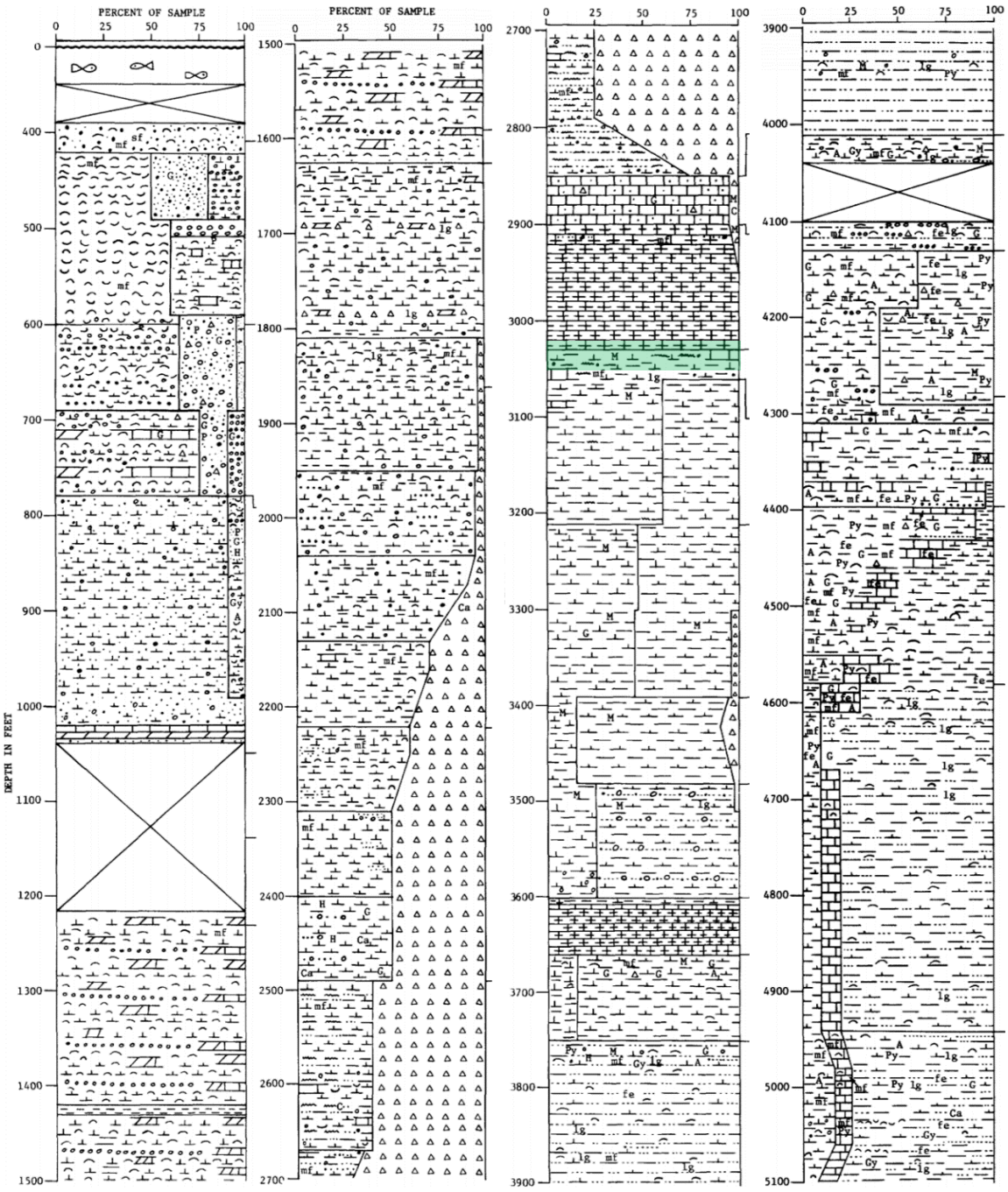

Figure A2: Lithologic log, COST GE-1 well, 0-5100 ft. Modified from Scholle (1979). Green highlighted portion indicates depth interval with available core at DGS.

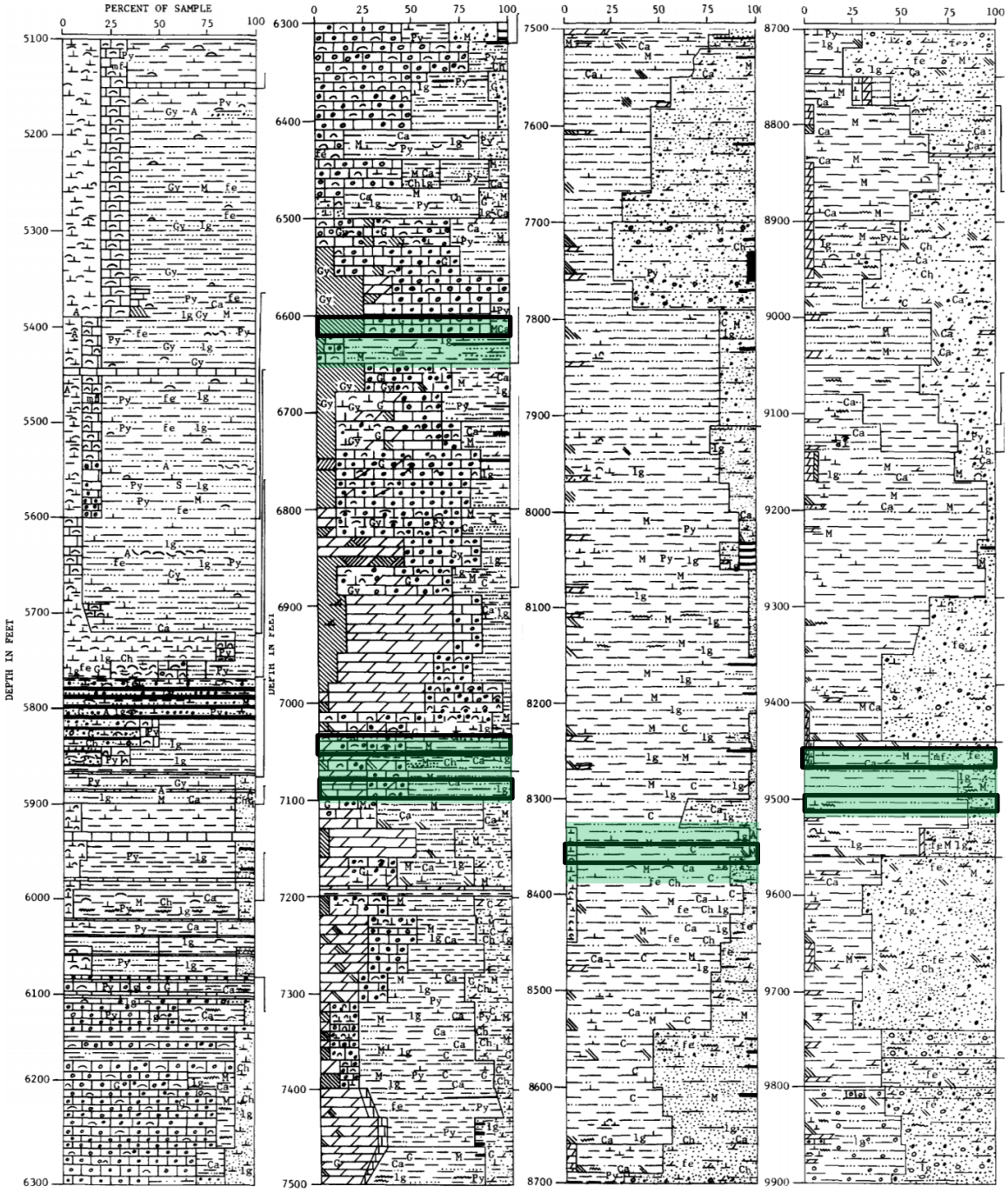

Figure A3: Lithologic log, COST GE-1 well, 5100-9900 ft. Modified from Scholle (1979). Green highlighted portion indicates depth interval with available core at DGS. Black outline indicates depth interval selected for study.

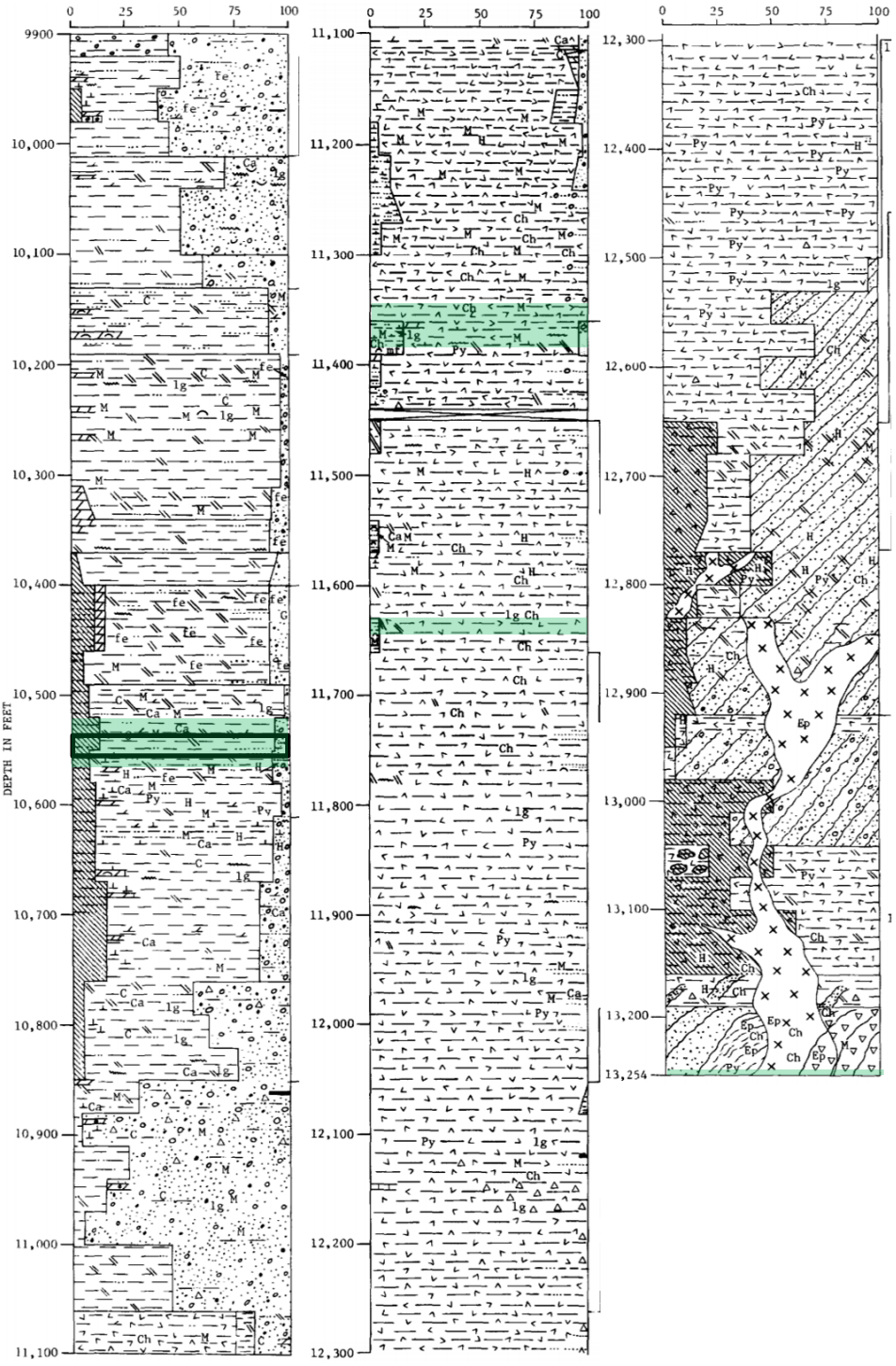

Figure A4: Lithologic log, COST GE-1 well, 9900-13254 ft. Modified from Scholle (1979). Green highlighted portion indicates depth interval with available core at DGS. Black outline indicates depth interval selected for study.

APPENDIX B

Core Photographs & Medical CT Scans

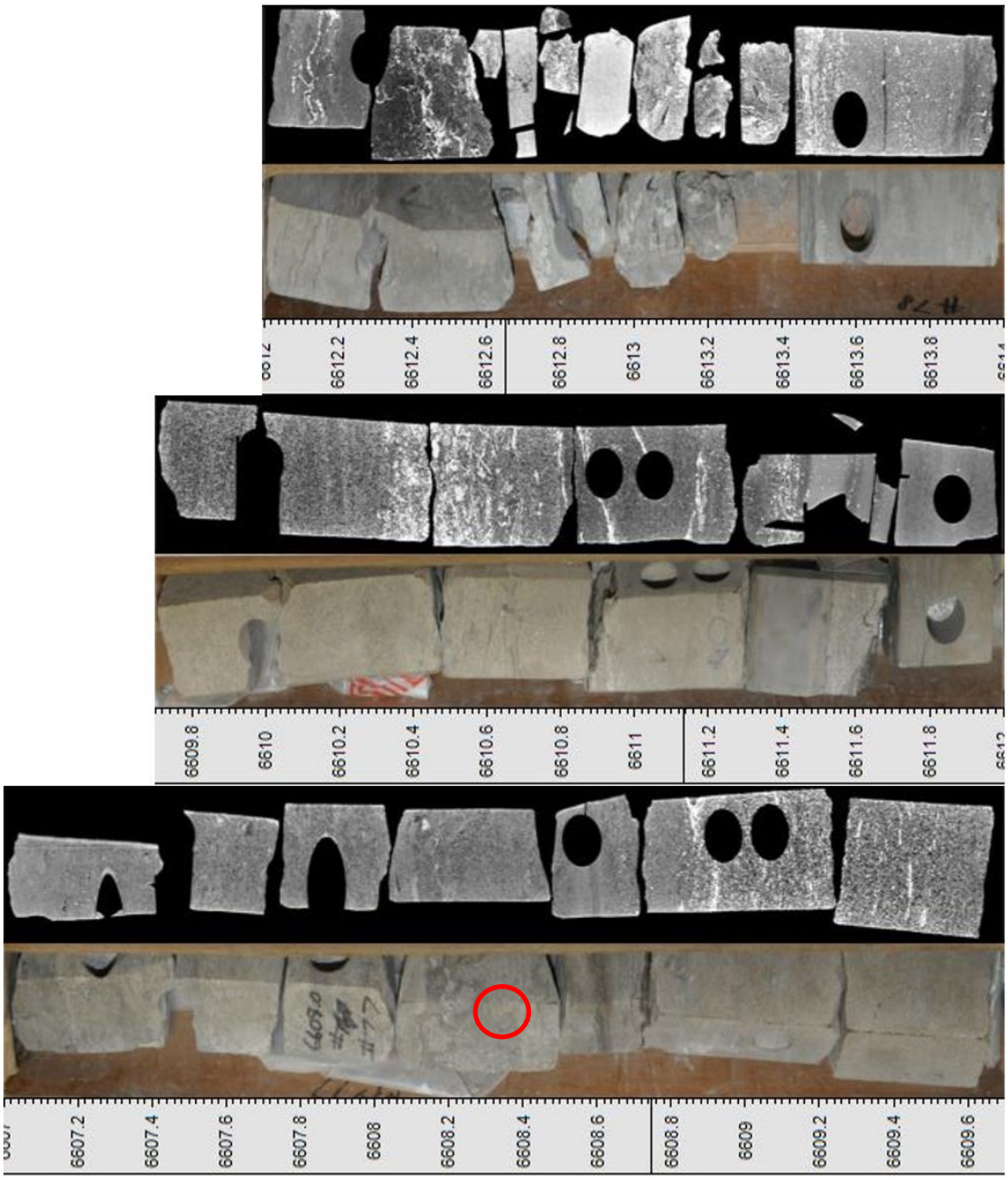

Figure A5: Depth interval 6607 ft (bottom) to 6614 ft (top) sampled from DGS. White light photographs and medical CT images are depth-aligned, and depths of plugs sampled are indicated with a red circle.

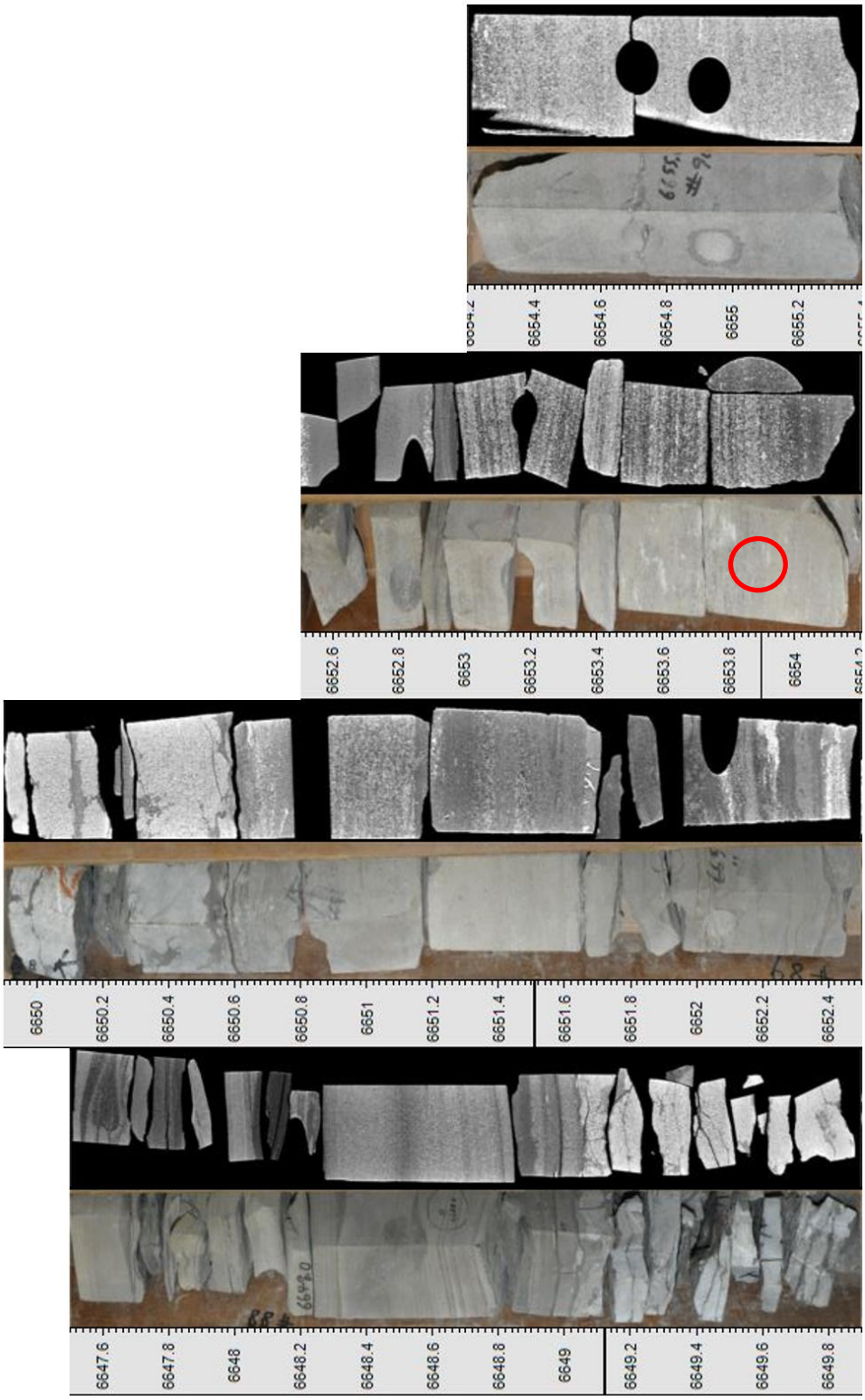

Figure A6: Depth interval 6647.5 ft (bottom) to 6655.4 ft (top) sampled from DGS. White light photographs and medical CT images are depth-aligned, and depths of plugs sampled are indicated with a red circle.

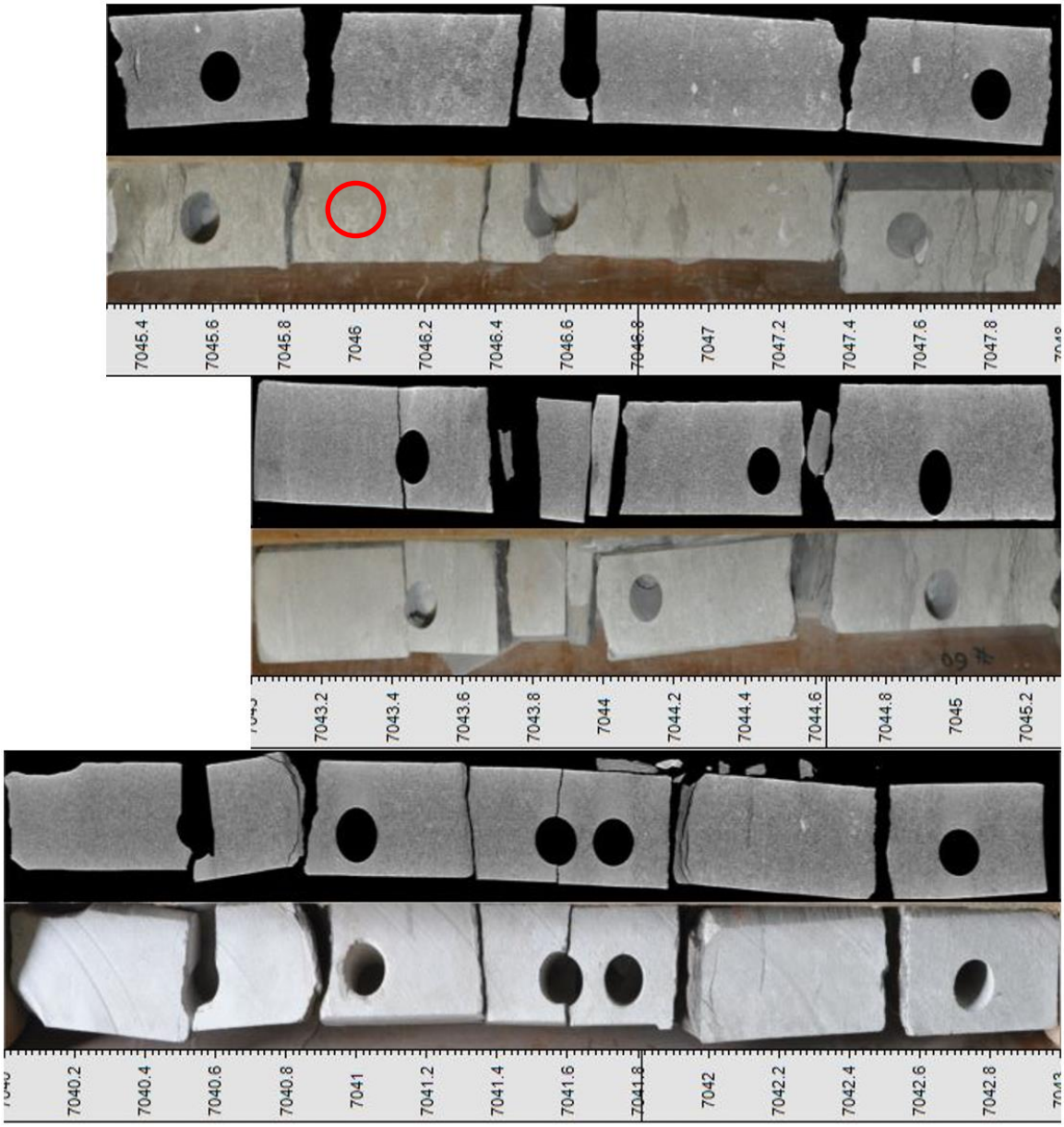

Figure A7: Depth interval 7040 ft (bottom) to 7048 ft (top) sampled from DGS. White light photographs and medical CT images are depth-aligned, and depths of plugs sampled are indicated with a red circle.

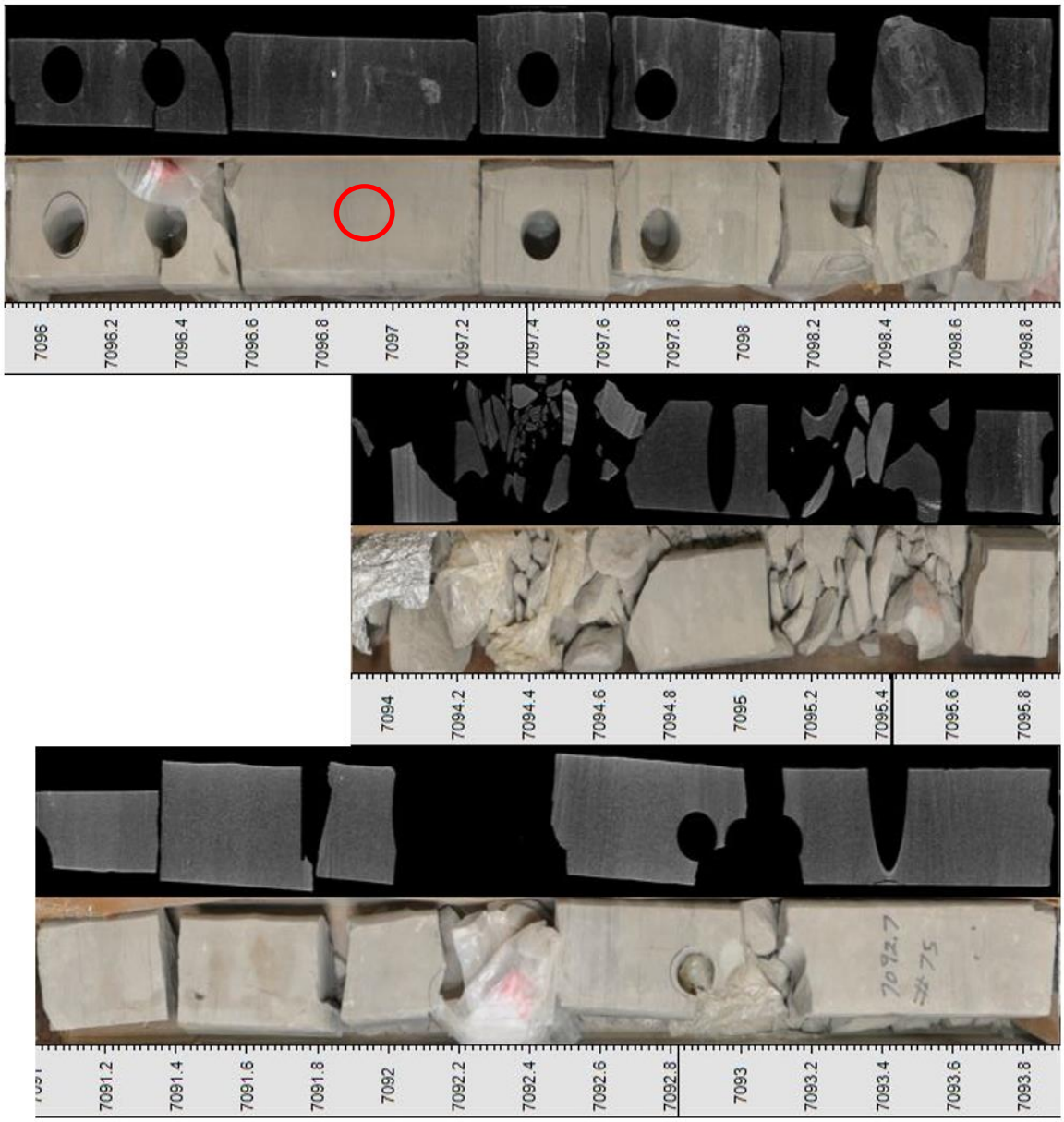

Figure A8: Depth interval 7091 ft (bottom) to 7098.9 ft (top) sampled from DGS. White light photographs and medical CT images are depth-aligned, and depths of plugs sampled are indicated with a red circle.

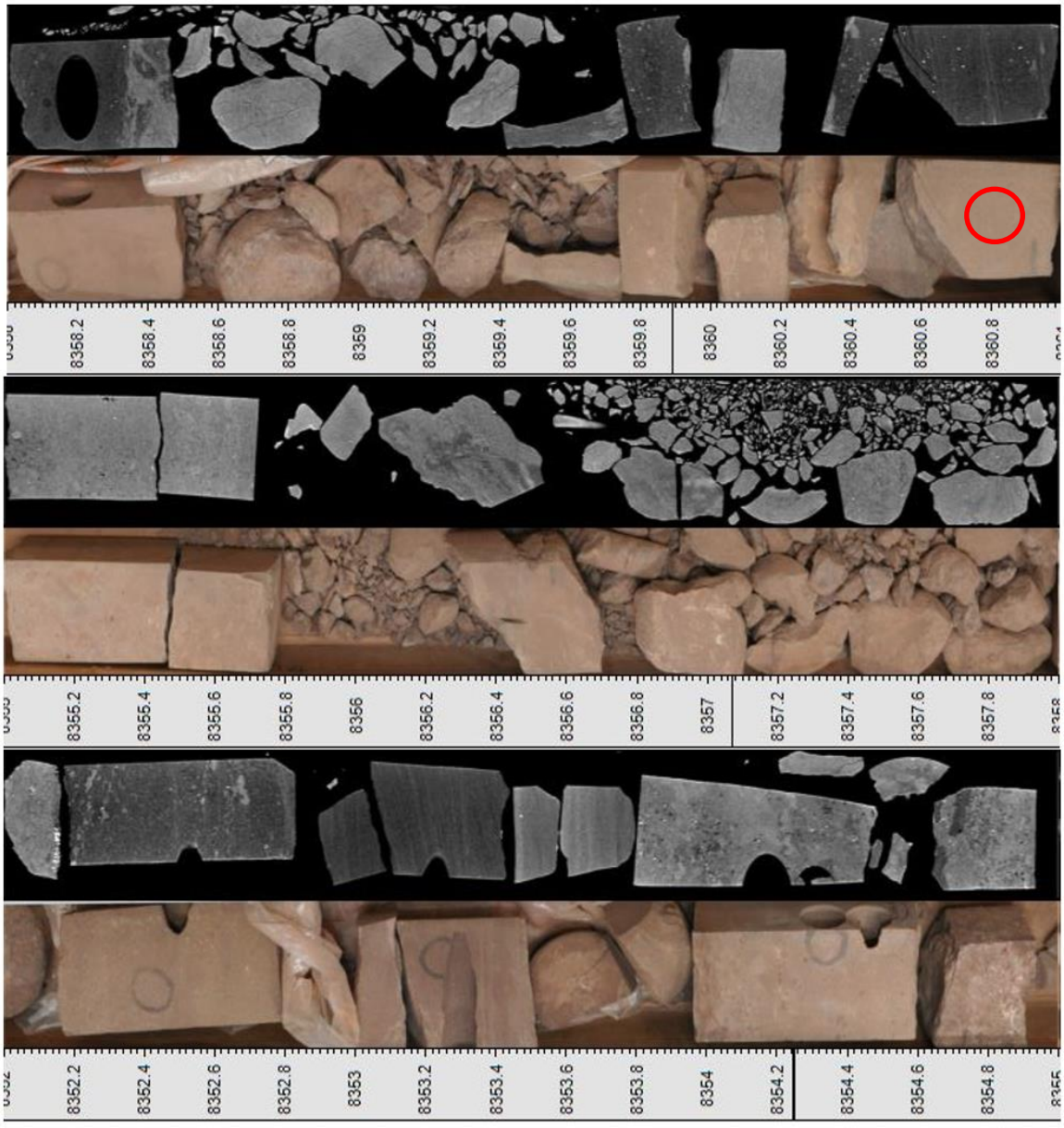

Figure A9: Depth interval 8352 ft (bottom) to 8361 ft (top) sampled from DGS. White light photographs and medical CT images are depth-aligned, and depths of plugs sampled are indicated with a red circle.

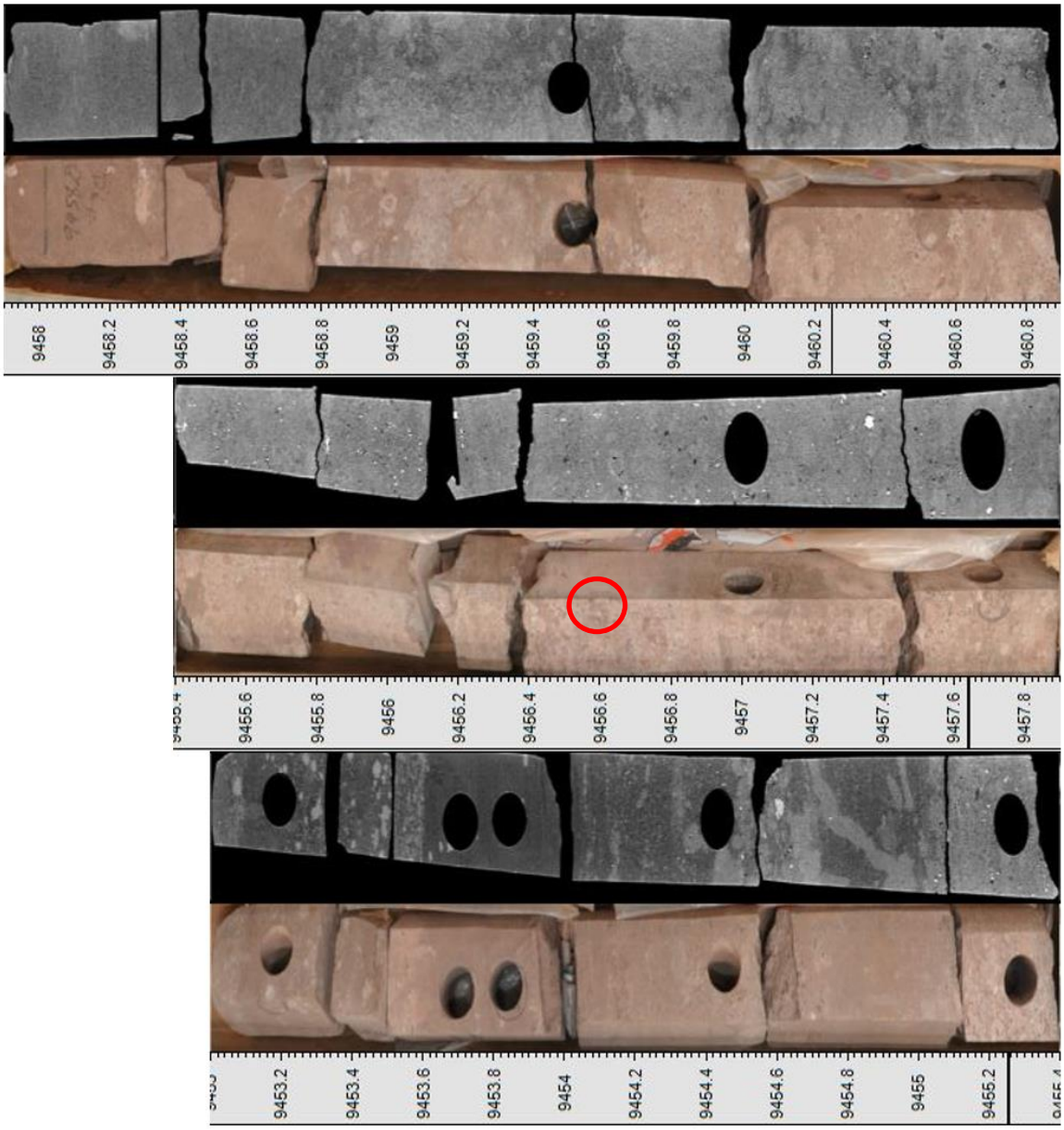

Figure A10: Depth interval 9453 ft (bottom) to 9460.9 ft (top) sampled from DGS. White light photographs and medical CT images are depth-aligned, and depths of plugs sampled are indicated with a red circle.

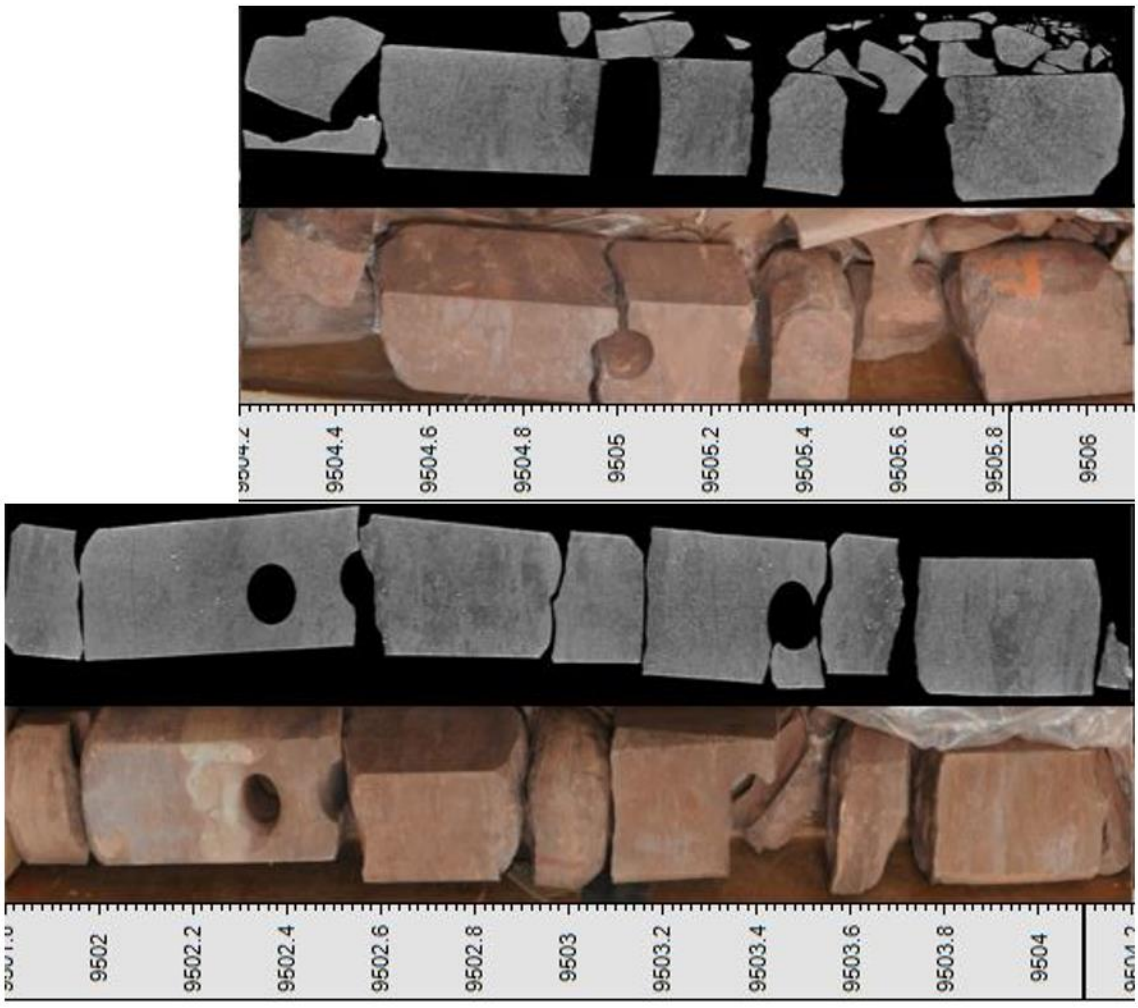

Figure A11: Depth interval 9501.8 ft (bottom) to 9506.1 ft (top) sampled from DGS. White light photographs and medical CT images are depth-aligned.

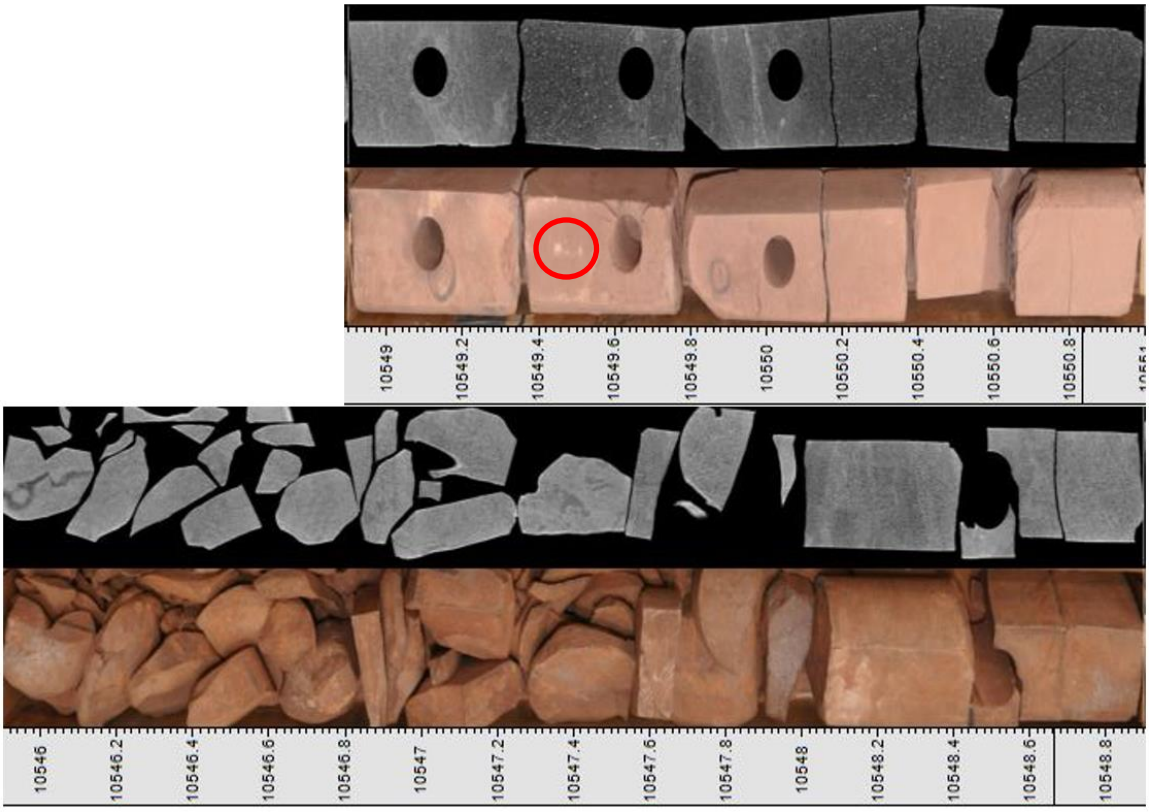

Figure A12: Depth interval 10545.9 ft (bottom) to 10551 ft (top) sampled from DGS. White light photographs and medical CT images are depth-aligned, and depths of plugs sampled are indicated with a red circle.

APPENDIX C

Industrial CT Scans

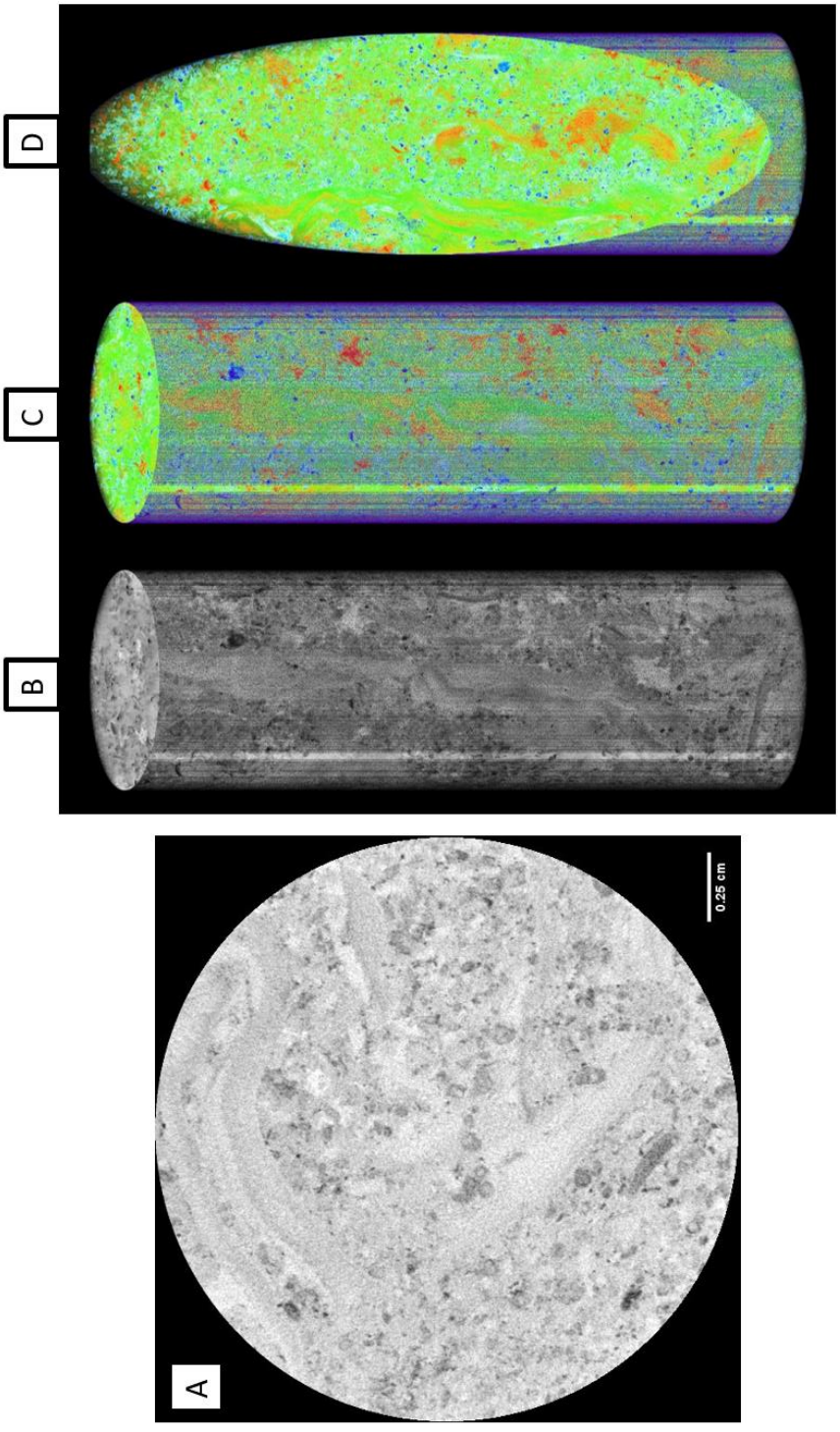

Figure A13: Industrial CT representations of plug 6608.5. [A] 2D horizontal slice in grayscale. [B] 3D volume in grayscale. [C] 3D volume with Thermal LUT filter applied highlighting density heterogeneities with less dense in blue to most dense in red. [D] A diagonal slice through C displaying interior structure.

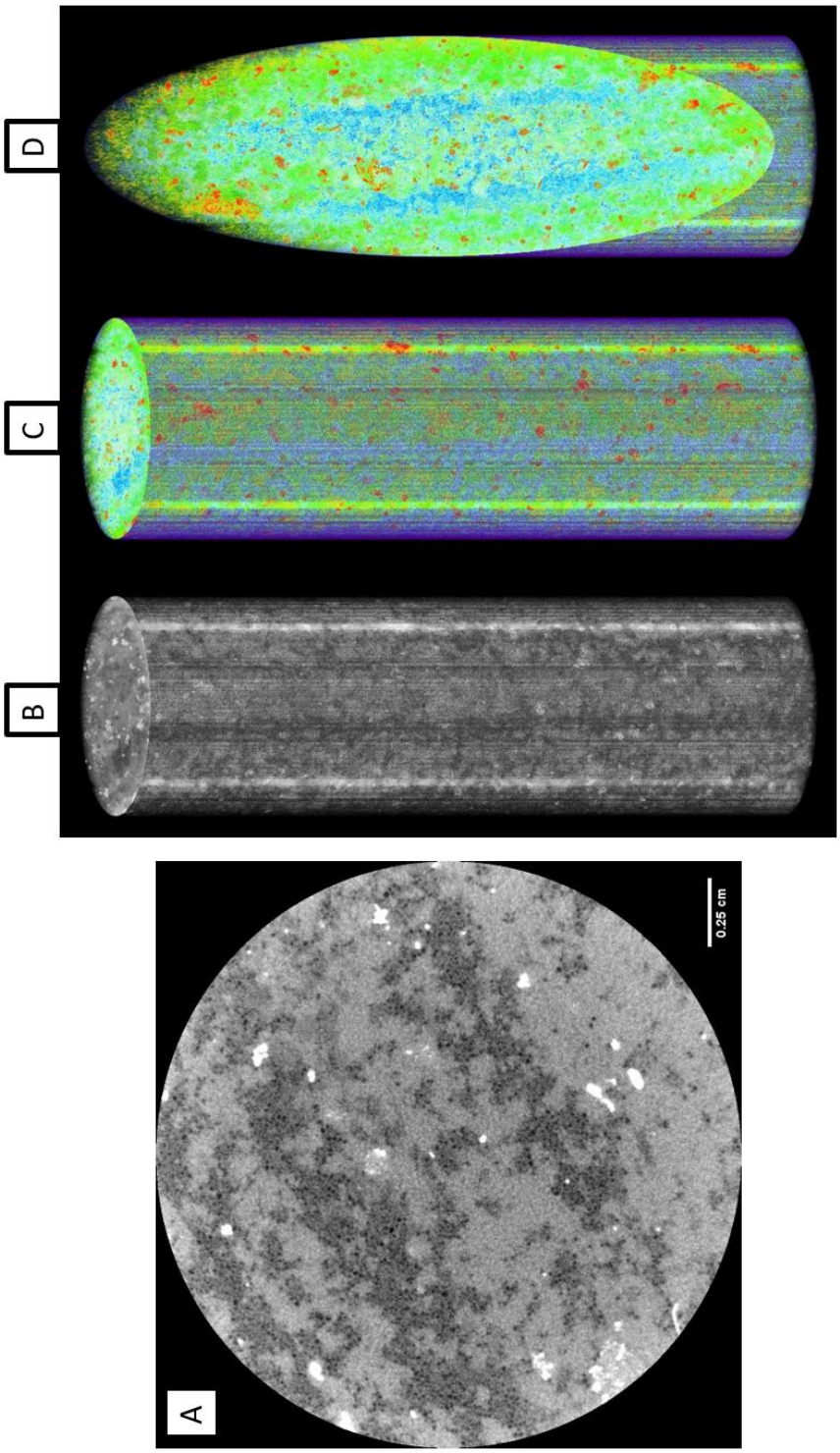

Figure A14: Industrial CT representations of plug 6654. [A] 2D horizontal slice in grayscale. [B] 3D volume in grayscale. [C] 3D volume with Thermal LUT filter applied highlighting density heterogeneities with less dense in blue to most dense in red. [D] A diagonal slice through C displaying interior structure.

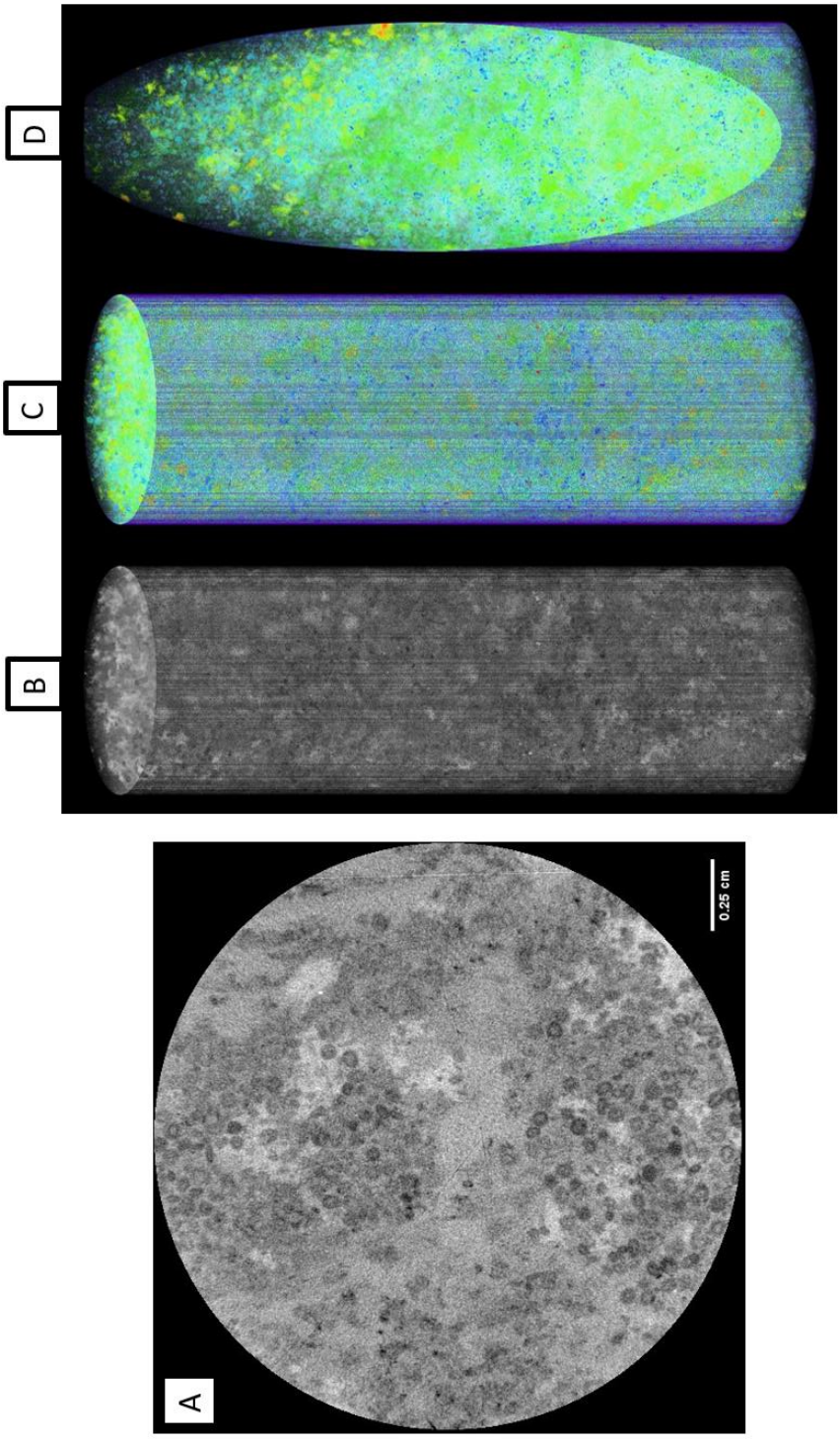

Figure A15: Industrial CT representations of plug 7046. [A] 2D horizontal slice in grayscale. [B] 3D volume in grayscale. [C] 3D volume with Thermal LUT filter applied highlighting density heterogeneities with less dense in blue to most dense in red. [D] A diagonal slice through C displaying interior structure.

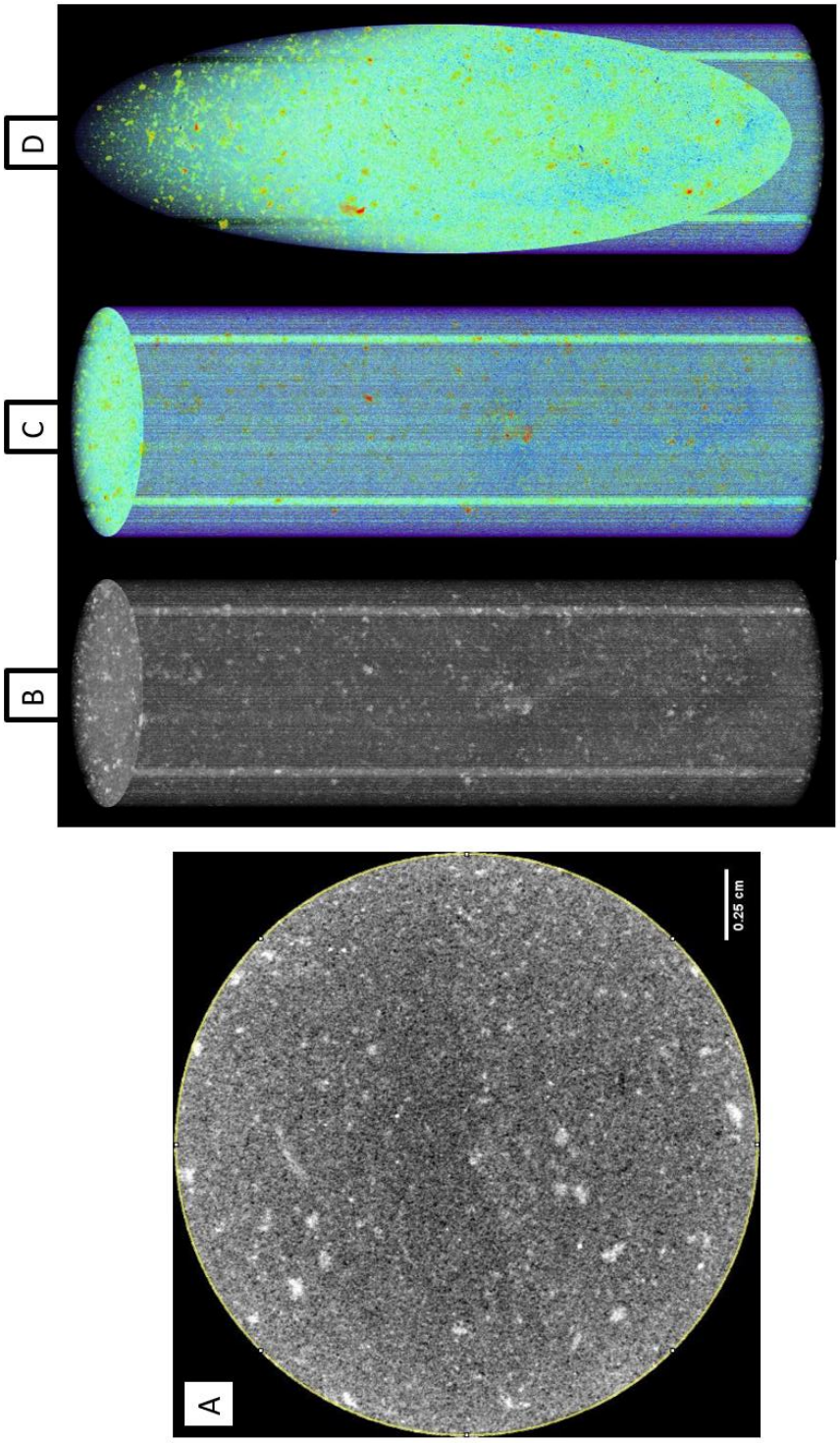

Figure A16: Industrial CT representations of plug 7096.9. [A] 2D horizontal slice in grayscale. [B] 3D volume in grayscale. [C] 3D volume with Thermal LUT filter applied highlighting density heterogeneities with less dense in blue to most dense in red. [D] A diagonal slice through C displaying interior structure.

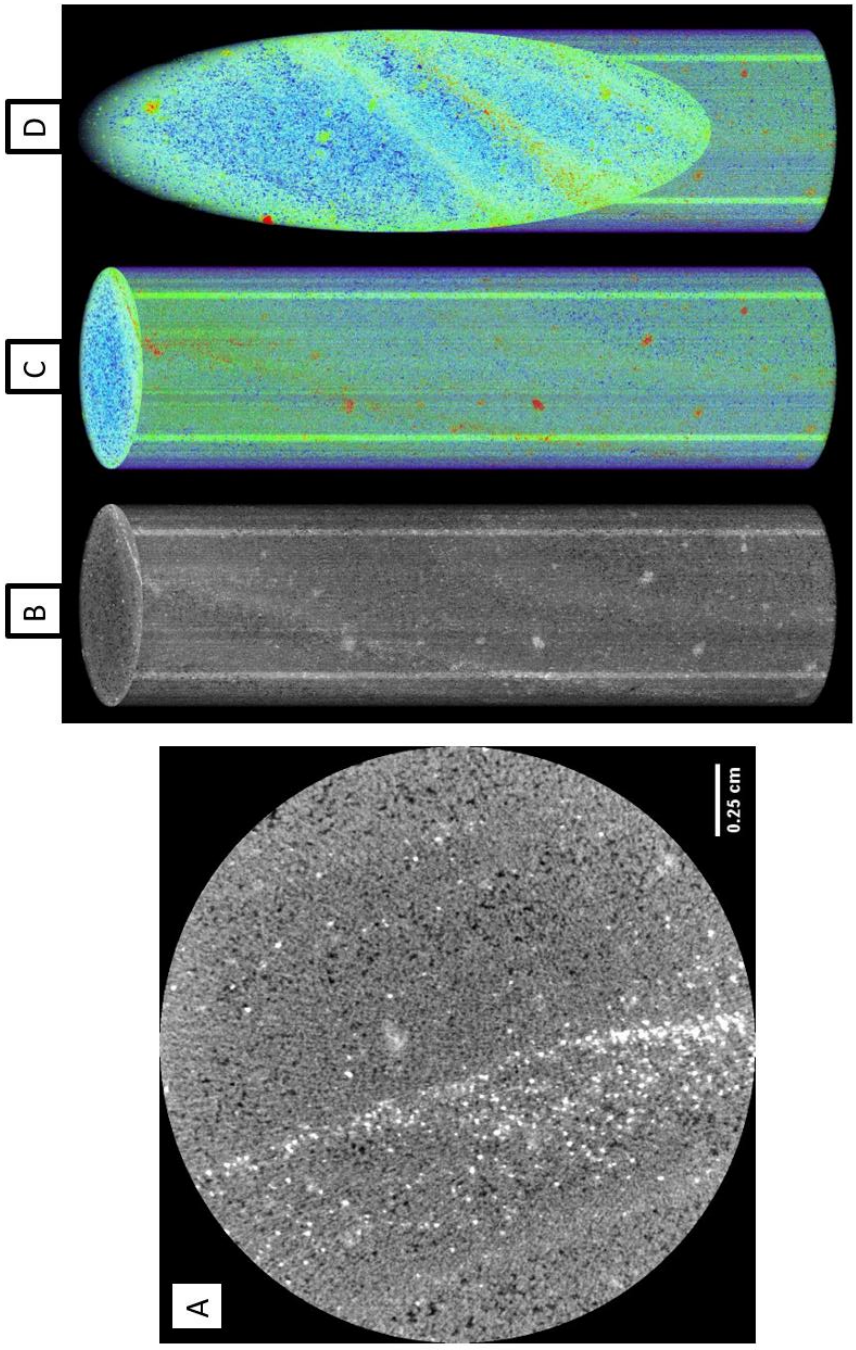

Figure A17: Industrial CT representations of plug 8360.5. [A] 2D horizontal slice in grayscale. [B] 3D volume in grayscale. [C] 3D volume with Thermal LUT filter applied highlighting density heterogeneities with less dense in blue to most dense in red. [D] A diagonal slice through C displaying interior structure.

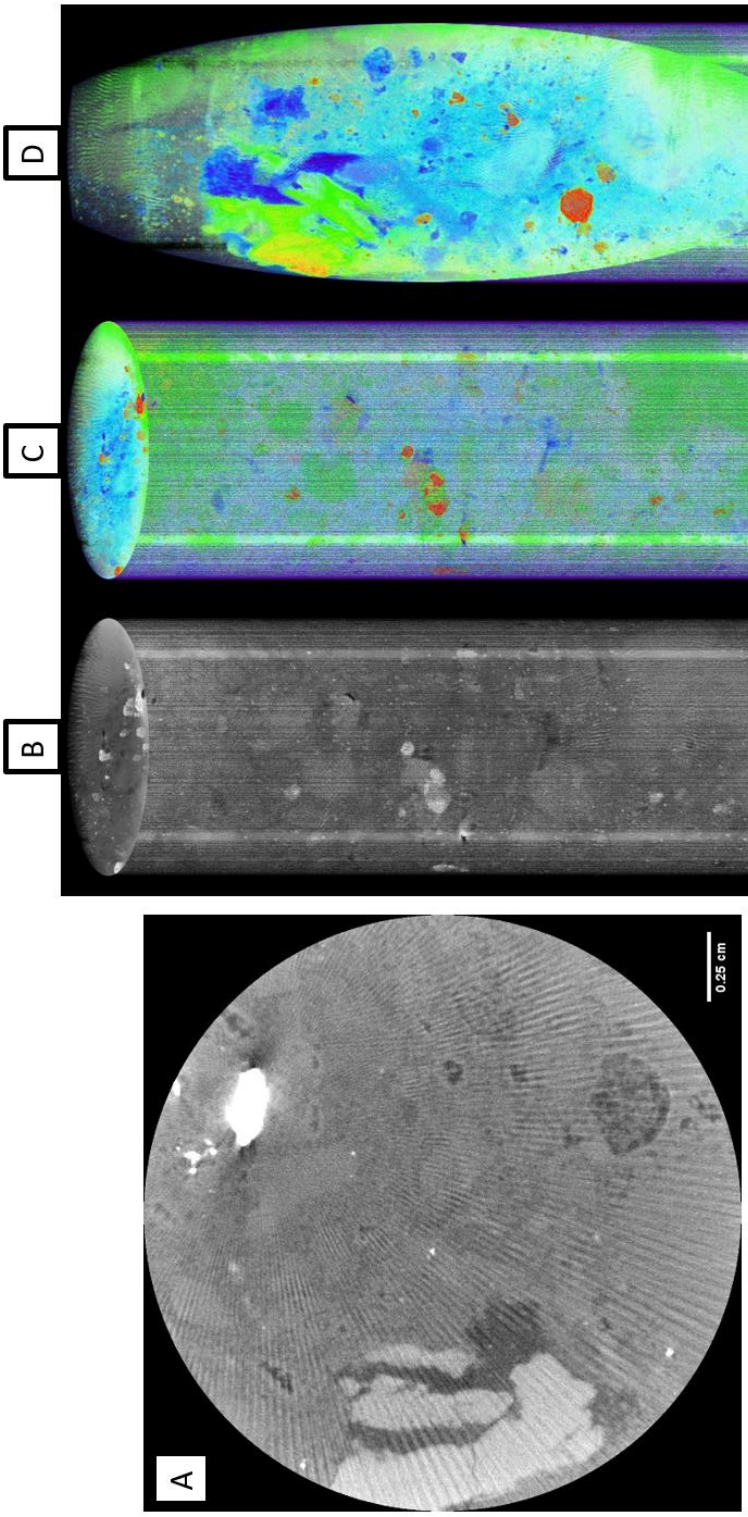

Figure A18: Industrial CT representations of plug 9456.4. [A] 2D horizontal slice in grayscale. [B] 3D volume in grayscale. [C] 3D volume with Thermal LUT filter applied highlighting density heterogeneities with less dense in blue to most dense in red. [D] A diagonal slice through C displaying interior structure.

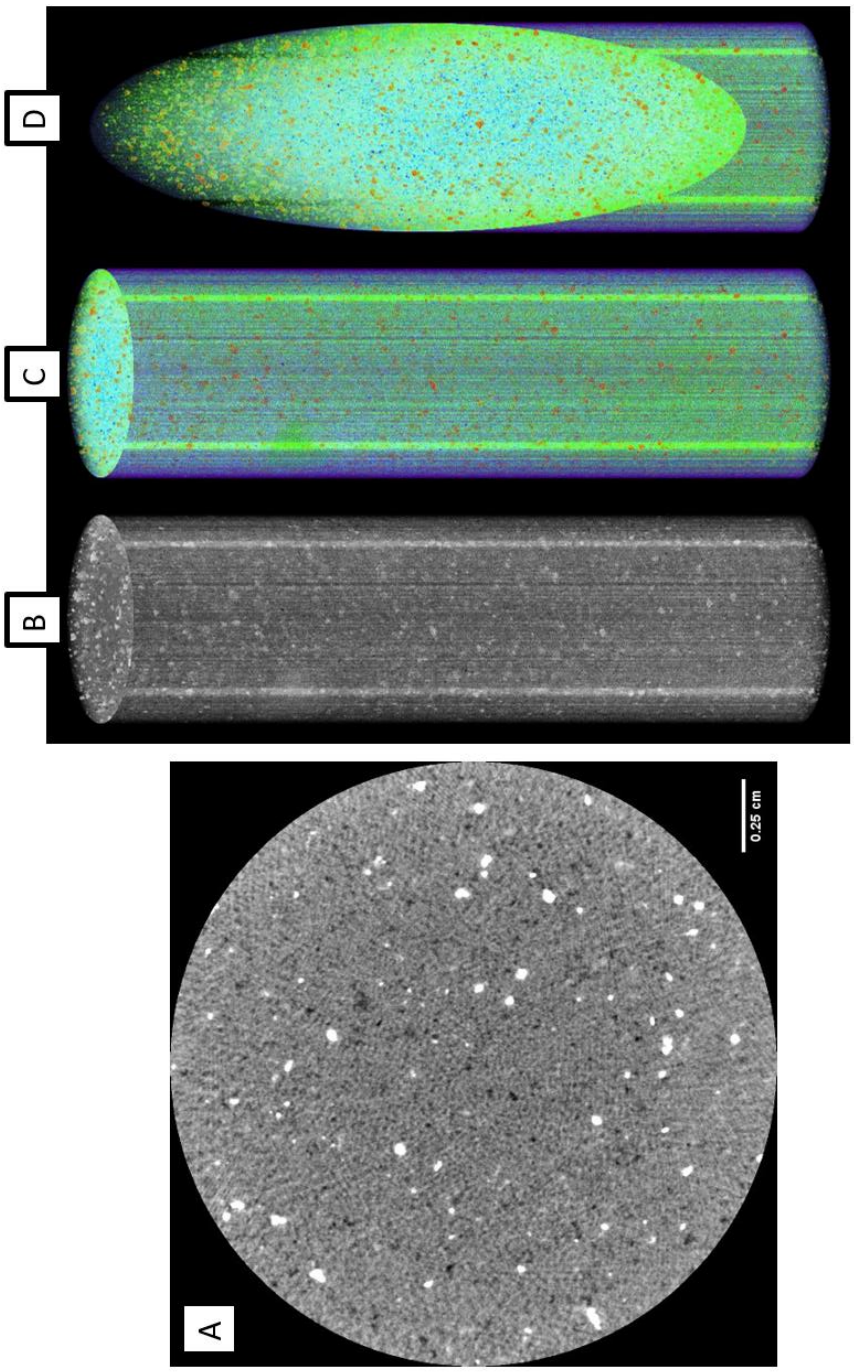

Figure A19: Industrial CT representations of plug 10550. [A] 2D horizontal slice in grayscale. [B] 3D volume in grayscale. [C] 3D volume with Thermal LUT filter applied highlighting density heterogeneities with less dense in blue to most dense in red. [D] A diagonal slice through C displaying interior structure.

VITA

Andrew Jacob Bean

Candidate for the Degree of

Master of Science

Thesis: ROCK PHYSICS CHARATCERIZATION OF POTENTIAL RESERVOIRS AND SEALS FOR CO2 STORAGE, OFFSHORE SOUTHEASTERN U.S.

Major Field: Geology

Education:

Completed the requirements for the Master of Science in Geology at Oklahoma State University, Stillwater, Oklahoma in July 2020.

Completed the requirements for the Bachelor of Science in Geology at West Virginia University, Morgantown, West Virginia in August 2016.

Completed the requirements for the Bachelor of Arts in Geography at West Virginia University, Morgantown, West Virginia in August 2016.

Experience:

Geotechnical Intern at Geo-Technology Associates, Inc., Abingdon, MD, 2014
Mickey Leland Energy Fellow at NETL, Morgantown, WV, 2015
Research Geologist Fellow at NETL, Morgantown, WV, 2015-2017
Geophysics Intern at NextEra Energy, Tulsa, OK, 2018
Petrophysics Intern at ConocoPhillips, Houston, TX, 2019
Petroleum Geologist at Battelle Memorial Institute, Albany, OR 2019-Present

Professional Memberships:

American Association of Petroleum Geologists
Society of Exploration Geophysicists
Geophysical Society of Oklahoma City
Houston Geological Society